https://ntrs.nasa.gov/search.jsp?R=19670030349 2020-03-24T00:01:58+00:00Z

Unclassified

Tech. Report No. 5

Some Aspects of the Deformation of a Neo-Hookean Material in Compression

D. Thompson and M. G. Sharma

July 1967

JPL Contract No. 950875

This work was performed for the Jet Propulsion Laboratory, California Institute of Technology sponsored by the National Aeronautics and Space Administration under Contract NAS 7 - 100

The Pennsylvania State University
University Park, Pennsylvania

Interim Report - II

GPO PRICE $

CFSTI PRICE(S) $

Hard copy (HC) 3.00

Microfiche (MF)

ff 653 July 65

FACILITY FORM 602

N67-39678 (ACCESSION NUMBER)

100 (PAGES)

CR-84586 (NASA CR OR TMX OR AD NUMBER)

(THRU)

1 (CODE)

32 (CATEGORY)

Unclassified

Tech. Report No. 5

Some Aspects of the Deformation of a Neo-Hookean Material in Compression

D. Thompson and M. G. Sharma

July 1967

JPL Contract No. 950875

This work was performed for the Jet Propulsion Laboratory, California Institute of Technology sponsored by the National Aeronautics and Space Administration under Contract NAS 7-100

The Pennsylvania State University
University Park, Pennsylvania

Interim Report - II

Preface

This is the fifth technical report covering the research work under the project entitled "A Test Program to Determine the Mechanical Behavior of Solid Propellants". The work reported here particularly refers to experimental studies on a rubber-like material that has been subjected to a uniaxial compression. The strains on the surface of a cylindrical specimen under given loads were measured via the moiré method of strain analysis. The boundary conditions on the ends of the cylinders were varied by varying the friction between the ends of the cylinders and the compression plates.

Abstract

Experiments were conducted by compressing, uniaxially, a series of cylinders of length to diameter ratio of two. The boundary conditions at the ends of the cylinders were varied with respect to the amount of friction present. The cylinders were cast of Solithane 113, a rubber-like material. The compressive stresses applied varied from 0 to 19.1 lb/in^2, for stresses which were based on the original cross-sectional area. Strains were measured on the surfaces of the cylinders, which corresponded to ten different values of applied stress. Strain was measured in the axial and circumferential directions by using the moire? fringe method. A short series of tension experiments were also conducted in order to verify the accuracy of the moiré fringe method as employed for this presentation.

A theoretical analysis was performed. The classical elastic solution to the problem of uniaxial compression of a cylinder has been done and is presented here in detail. A short review of the finite deformation of a cylinder of Neo-Hookean material under uniaxial compression which produces bulging is given.

The theoretical strains as predicted by the classical theory are compared to the experimentally determined strains. A comparison of the strains obtained experimentally with different boundary conditions is presented. Also, a comparison of the stress-strain curves for Solithane in compression and tension is given.

Table of Contents

Page

Preface. i

Abstract ii

List of Tables iv

List of Figures v

List of Symbols vi

Chapter 1. Introduction

1. Statement of the Problem 1
2. Importance of the Investigation. 2
3. Scope and Limitations 3

Chapter 2. Theoretical Investigation

1. Solution of the Problem by Classical Elasticity Theory . 7
2. Review of Finite Deformation Theory 26
3. Finite Deformation Theory Appliedto the Problem . . . 31
4. Predictions of the Strains by the Theory. 38

Chapter 3. Experimental Investigation

1. Description of the Material 42
2. Specimen Preparation 42
3. Experimental Apparatus and Procedure 45
4. Moiré Fringe Theory 51

Chapter 4. Experimental Results and Discussion

1. Tension Experiments 61
2. Compression Experiments 62
3. Conclusions 63
4. Suggestions for Further Research 64

References. 65

Appendix A (Mathematical Calculations) 66

Appendix B (Diazo Solution and Printing Process) 74

Appendix C (Sample Analysis of Moiré Fringes) 76

List of Tables

Table		Page
2.4.1.	Theoretical Circumferential Strain for Various Values of Applied Load.	41
2.4.2.	Theoretical Axial Strain for Various Values of Applied Load.	41
4.1.1	Experimentally Determined Values of Moduli *for* Different Specimens	62

List of Figures

Figure		Page
1	Definition of Coordinate System used in Theoretical. Derivations.	77
2	Molds for Casting Cylindrical Specimens	78
3	Curing Oven.	79
4	Tinius Olsen Testing Machine with Compression Apparatus Installed	80
5	Tension Specimen	81
6	Tension Specimen Grips	81
7	Compression Specimen.	82
8	Close Up of Formation of Moire Fringes.	83
9	Moire Fringe Analysis by Displacement	84
10	Sample Output of Photocell Equipment of Light Intensity Method	85
11	Compressive Load Versus True Circumferential Strain for Non-Lubricated Ends.	86
12	Compressive Load Versus True Circumferential Strain for Lubricated Ends	87
13	Compressive Load Versus True Axial Strain for Non-Lubricated Ends	88
14	Compressive Load Versus True Axial Strain for Lubricated Ends	89
15	True Stress Versus Nominal Strain	90
16	Moiré Fringes	91
17	Accumulated Fringe Distance Versus Fringe Number	92
18	True Stress Versus True Strain for Determination of Modulus.	93

List of Symbols

a	radial distance to outside of cylinder
c	one-half of the length of the cylinder
D^2	operator denoting $\frac{\partial^2}{\partial z^2}$
E	Young's modulus
ℓ^2	operator denoting $\frac{d}{dr}\frac{1}{r}\frac{d}{dr}r$
$I_0(kr)$	modified Bessel function of the first kind of zero order
$I_1(kr)$	modified Bessel function of the first kind of order one
$K_0(kr)$	modified Bessel function of the second kind of zero order
$K_1(kr)$	modified Bessel function of the second kind of order one
k	separation of variables constant
p	hydrostatic pressure
Q	total normal pressure applied to each end of the cylinder
r	coordinate in the radial direction
$R(r)$	function of r only, used in separation of variables method
R_I	body force in the r direction
R_ν	stress acting on the boundary in the r direction
u	displacement in the r direction
u_o	constant of integration
v	displacement in the θ direction
w_o	constant of integration
w	displacement in the z direction
z	coordinate in the axial direction
$Z(z)$	function of z only, used in the separation of variables method
Z_I	body force in the z direction

Z_ν	stress acting on the boundary in the z direction
a	denotes "ka"
γ	constant equaling $\frac{\lambda+\mu}{\lambda+2\mu}$
θ	coordinate perpendicular to r and z
$\theta(z)$	constant of integration
Θ	*body* force in θ direction
λ	Lamé's constant
μ	Lamé's constant
ρ	denotes "kr"
ρ_o	density of material
σ_{ij}	stress in the j direction on the i plane
τ	volume
ϕ	coordinate perpendicular to r and z
$\chi(r)$	constant of integration

CHAPTER 1

INTRODUCTION

1.1 Statement of the Problem

In recent years much attention has been drawn to new classes of materials. One important class, the rubber-like material, is already in wide use. As an example, solid fuel propellants are placed in this category. Certain rubber-like materials are also used as vibration dampers. In order to construct reliable engineering structures, it is important to know just how a class of materials will deform under a given system of loads and with given boundary conditions.

The subject of this presentation is the study of a rubber-like material subjected to a uniaxial compressive load. Experimentally, a right, circular cylinder with length to diameter ratio of two is considered. The boundary conditions are with respect to the amount of friction present at the plane ends of the cylinder where the load application occurs. The axial and circumferential strains on the surface of the cylinder at its axial center are measured as the load varies from zero to sixty pounds, in increments of six pounds. The end boundary conditions are also varied from one experiment to the next, i.e., the amount of friction between the end plates and the specimen ends is varied by the application of a lubricant.

A relatively new method of strain measurement, the moiré method, is employed, Therefore, tension experiments designed to measure modulus were also conducted and the results, using the moire method, are compared to the results of previously conducted tension experiments where clip gages had been used for strain measurement. This comparison

is made in order to verify the accuracy of the moiré fringe method of strain measurement, as used here.

An attempt to solve the problem, theoretically, of the large deformation under uniaxial compression, of a right, circular cylinder of incompressible material is made. It is assumed that there is no slipping of the ends of the specimen with respect to the compression plates during an application of load. Due to mathematical intractabilities in the solution of the problem, no final solution is given in this discussion.

1.2 Importance of the Investigation

A study of the aforementioned problem is necessitated by several things. As has been mentioned, many so-called rubber-like materials are now in existence and, conceivably, many more will be developed in the future. In order to design reliable structures with a minimum of material and cost, and having a maximum of safety, the material properties of the design material must be known.

With regard to this specific problem, compression is surely one of the important loading configurations to be considered in most design problems. For instance, the solid fuel propellant in a rocket sometimes has the shape of a thick-walled cylindrical tube. The burning of the fuel proceeds from the inner wall to the outer wall. With this burning, there exists high temperatures and pressures. These high temperatures and pressures exert compressive forces on the wall of the cylindrical tube. As can be seen by this example, compression is an important loading configuration and this importance warrants further study of the problem.

1.3 Scope and Limitations

The work presented here delves into one aspect of the problem of compression of materials. The geometrical shape of the body being considered, the manner in which the load is being applied, the boundary conditions being imposed, and the type of material being considered all contribute to the limitations of the scope of the problem, both experimentally and theoretically.

A right, circular cylinder, with the length being twice the diameter, will be considered, both experimentally and theoretically. This length to diameter ratio is chosen in order to facilitate good bulging of the curved surface of the cylinder. A cylindrical shape, instead of a parallelepiped, is chosen solely for reasons of theoretical simplicity. A parallelepiped would yield infinite stresses at its edges.

A uniaxial compressive load is applied to the terminal ends of the cylinder in both the theoretical and experimental investigations. In the theoretical case, the total load is assumed to be known, however, the manner in which this load is distributed over the end surfaces is unknown, except that at the edge of each surface the load must be zero. Also, the total load applied is considered in the experimental investigation. The total load is varied from zero to sixty pounds and the strains are determined experimentally and theoretically at increments of six pounds.

For the theoretical case, the boundary conditions assumed are as follows. A given total stress acts on the ends. No axial or circumferential stresses exist on the curved surface of the cylinder. A

shear stress of unknown distribution acts on each end in order to constrict the ends from axial movement as the load is applied. Also, the ends are constrained to remain plane when the load is applied.

For the experimental case, one of the boundary conditions is varied fromthat in the theoretical case. A given total stress is applied to the ends as previously mentioned. Also, no axial or circumferential stresses exist on the curved surface. The ends are constrained to remain plane as the load is applied. But, the shear stress on the end is not always the same as in the theoretical case. Two cases are considered. The ends are constricted from axial movement in one case. In the other case, there is some amount of axial movement of the ends for a given load.

In the theoretical case, the material is considered to be Neo-Hookean. A Neo-Hookean material is one that obeys a type of stress-strain relationship that is shown to be a natural extension of the Hooke's law used in the study of small elastic deformations. The material is also assumed to be homogeneous, isotropic, and incompressible.

Experimentally, the material considered is similar, in some aspects, to that assumed for the theoretical treatment. The material used, Solithane II3, is homogeneous and isotropic. As to whether Solithane II3 is incompressible and a Neo-Hookean material is still unknown.

Chapter Two deals with the theoretical investigation. Part One is a study of the classical elasticity solution to the problem of a cylinder of moderate length being compressed uniaxially with given

boundary conditions as derived by Filon (3). Section Two of Chapter Two is a short review of the finite deformation theory as presented by Rivlin (6). The basic equations of this theory are set forth and include the stress versus deformation equations, the incompressibility condition, the equations of equilibrium, et al. Part Three of this chapter is an application of the finite deformation theory to the specific problem dealt with in this presentation. Part Four sets forth the results of the calculations of the surface strains as predicted by the classical elasticity theory.

The experimental investigation is described in Chapter Three. A chemical description of the material used in the experimental program is given in Section One of Chapter Three. Part Two of this chapter deals with the exact manner in which the specimens that were used in the experimental investigations were made. The procedure used in testing the specimens is described in Part Three of this chapter. Also in this part, one will find a description of the various apparatus used in the experimental program. Part Four describes the theory behind the moiré method of strain analysis. This description includes a short review of three of the most common methods of analyzing moiré fringes along with a comparative analysis of the three different methods.

In Chapter Four the results of the experimental investigations are set forth. Data for both tension and compression experiments are presented. A comparison between the experimental results in compression, with the proper boundary conditions, and the theoretical results as given by the classical theory of elasticity is made. All

prevalent results of the experimental data *are* discussed in detail, and **conclusions** are drawn.

CHAPTER 2

THEORETICAL INVESTIGATION

2.1 Solution of the Problem by Classical Elasticity Theory

The following was taken from parts of a paper by L.N.G. Filon (3). The reasons for reproducing it here are two fold. First, as presented here, the solution of the problem is in much greater detail than in the original paper. Also, the problem, as solved by Filon, was studied in order to obtain some insight into the problem of the compression of a cylinder in general and the boundary conditions of that problem in particular.

The problem discussed is that of a cylinder of moderate length, when compared to the diameter, which is compressed between two rigid planes in such a way that the terminal cross-sections are constrained to remain plane. In this section of the theoretical development, the general equations for the elastic case of a right, circular cylinder of finite length are obtained. The method adopted has been to obtain symmetrical solutions of the equations of elasticity in cylindrical coordinates and to express the typical term in the form $(\cos kz)xf(r)$ and $(\sin kz)xf(r)$.

Let us first consider the differential equations of equilibrium in cylindrical coordinates as shown by Timoshenko (9).

$$\frac{\partial \sigma_{rr}}{\partial r} + \frac{1}{r}\frac{\partial \sigma_{r\phi}}{\partial \phi} + \frac{\partial \sigma_{rz}}{\partial z} + \frac{\sigma_{rr} - \sigma_{\phi\phi}}{r} = 0$$

$$\frac{\partial \sigma_{rz}}{\partial r} + \frac{1}{r}\frac{\partial \sigma_{\phi z}}{\partial \phi} + \frac{\partial \sigma_{zz}}{\partial z} + \frac{\sigma_{rz}}{r} = 0$$

$$\frac{\partial \sigma_{r\phi}}{\partial r} + \frac{1}{r}\frac{\partial \sigma_{\phi\phi}}{\partial \phi} + \frac{\partial \sigma_{\phi z}}{\partial z} + \frac{2\sigma_{r\phi}}{r} = 0 \qquad (2.1.1)$$

Writing the stresses in terms of displacements and employing Lamé's constants

$$\begin{aligned}
\sigma_{rr} &= (\lambda + 2\mu)\frac{du}{dr} + \lambda\frac{u}{r} + \lambda\frac{dw}{dz} \\
\sigma_{zz} &= A\frac{du'}{dr} + (\lambda+2\mu)\frac{dw}{dz} + \lambda\frac{u}{r} \\
\sigma_{\phi\phi} &= (\lambda + 21.1)\frac{u}{r} + A\frac{du}{dr} + \lambda\frac{dw}{dz} \\
\sigma_{rz} &= \mu\left(\frac{dw}{dr} + \frac{du}{dz}\right) \\
\sigma_{\phi z} &= \mu\frac{dv}{dz} \\
\sigma_{r\phi} &= \mu\left(\frac{dv}{dr} - \frac{v}{r}\right) .
\end{aligned} \qquad (2.1.2)$$

Placing the stresses as written in equations (2.1.2) into the equilibrium equations (2.1.1), we obtain after rearranging and assuming that u, v, and w are independent of ϕ,

$$(\lambda+2\mu)\frac{d^2u}{dr^2} + (\lambda+2\mu)\frac{d}{dr}\left(\frac{u}{r}\right) + \mu\frac{d^2u}{dz^2} + (\lambda+\mu)\frac{d^2w}{drdz} - 0 \qquad (a)$$

$$\frac{d}{dr}\left[\frac{1}{r}\frac{d(rv)}{dr}\right] + \frac{d^2v}{dz^2} = 0 \qquad (b) \quad (2.1.3)$$

$$(\lambda+\mu)\left(\frac{d^2u}{drdz} + \frac{1}{r}\frac{du}{dz}\right) + \mu\left(\frac{d^2w}{dr^2} + \frac{1}{r}\frac{dw}{dr}\right) + (\lambda+2\mu)\frac{d^2w}{dz^2} = 0 . \qquad (c)$$

Let us define the operators

$$\ell^2 \equiv \frac{d}{dr}\frac{1}{r}\frac{d}{dr}r$$

and (2.1.4)

$$D \equiv \frac{d}{dz} .$$

Differentiating (2.1.3.a) with respect to z and (2.1.3.c) with respect to r.

$$(\lambda+2\mu)\frac{d}{dz}\left[\frac{d^2u}{dr^2}\right]+(\lambda+2\mu)\frac{d}{dz}\left[\frac{d}{dr}\left(\frac{u}{r}\right)\right]+\mu\frac{d}{dz}\left[\frac{d^2u}{dz^2}\right]+(\lambda+\mu)\frac{d}{dz}\left[\frac{d^2w}{drdz}\right]=0$$

and

$$(\lambda+\mu)\frac{d}{dr}\left[\frac{d^2u}{drdz}+\frac{1}{r}\frac{du}{dz}\right]+\mu\frac{d}{dr}\left[\frac{d^2w}{dr^2}+\frac{1}{r}\frac{dw}{dr}\right]+(\lambda+2\mu)\frac{d}{dr}\left[\frac{d^2w}{dz^2}\right]=0\ .$$

Rearranging and substituting equations (2.1.4).

$$\left[(\lambda+2\mu)\ell^2+\mu D^2\right]\frac{du}{dz}+(\lambda+\mu)D^2\frac{dw}{dr}=0 \qquad (2.1.5)$$

$$(\lambda+\mu)\ell^2\frac{du}{dz}+\left[\mu\ell^2+(\lambda+2\mu)D^2\right]\frac{dw}{dr}=0 \qquad (2.1.6)$$

and from equation (2.1.3.b)

$$(\ell^2+D^2)v=0. \qquad (2.1.7)$$

From equations (2.1.5) and (2.1.6) eliminate $\frac{du}{dz}$ and rearrange

$$\left[-(\lambda+\mu)^2\ell^2D^2\right]\frac{dw}{dr}+\left[(\lambda+2\mu)\mu\ell^4+(\lambda+2\mu)\mu D^4+\mu^2\ell^2D^2+(\lambda+2\mu)^2\ell^2D^2\right]\frac{dw}{dr}\equiv 0$$

$$\left[\left[(\lambda+2\mu)\mu\right]\ell^4+2\mu(\lambda+2\mu)\ell^2D^2+(\lambda+2\mu)\mu D^4\right]\frac{dw}{dr}=0$$

$$\left[\ell^4+2\ell^2D^2+D^4\right]\frac{dw}{dr}=0$$

$$(\ell^2+D^2)^2\frac{dw}{dr}=0=(\ell^2+D^2)^2y_1$$

Similarly, by eliminating $\frac{dw}{dr}$

$$(\ell^2+D^2)^2\frac{du}{dz}=0=(\ell^2+D^2)^2y_2\ .$$

The solution of this differential equation determines the elastic equilibrium of the circular cylinder under any symmetrical system of stresses.

The above differential equation can be solved by the separation of variables method. Consider first the equation $(\ell^2 + D^2)y = 0$. Let

$$y_3 = R_1(r)Z_1(z) .$$

$$(\ell^2 + D^2)R_1(r)Z_1(z) = 0$$

$$\left[\frac{d^2}{dr^2} + \frac{1}{r}\frac{d}{dr} - \frac{1}{r^2} + \frac{d^2}{dz^2}\right]R_1(r)Z_1(z) = 0$$

$$1\frac{d^2R_1}{dr^2} + Z_1\frac{1}{r}\frac{dR_1}{dr} - \frac{R_1Z_1}{} + R_1\frac{d^2Z_1}{dz^2} = 0$$

Dividing by Z_1R_1 to separate the variables.

$$\frac{1}{R_1}\frac{d^2R_1}{dr^2} + \frac{1}{R_1r}\frac{dR_1}{dr} - \frac{1}{r^2} + \frac{1}{Z_1}\frac{d^2Z_1}{dz^2} = 0$$

Rearranging

$$\frac{1}{R_1}\frac{d^2R_1}{dr^2} + \frac{1}{R_1r}\frac{dR_1}{dr} - \frac{1}{r^2} = -\frac{1}{Z_1}\frac{d^2Z_1}{dz^2} = +k^2 .$$

Separating the equation

$$\frac{1}{R_1}\frac{d^2R_1}{dr^2} + \frac{1}{R_1r}\frac{dR_1}{dr} - \frac{1}{r^2} = +k^2$$

$$\frac{1}{Z_1}\frac{d^2Z_1}{dz^2} = -k^2.$$

Rearranging

$$\frac{d^2R_1}{dr^2} + \frac{1}{r}\frac{dR_1}{dr} - \left(\frac{1}{r^2} + k^2\right) R_1 = 0 \qquad (2.1.8)$$

whose solution is

$$\underline{R_1 = AI_1(\kappa r) + BK_1(kr)}$$

$$\frac{d^2Z_1}{dz^2} + k^2Z_1 = 0 \qquad (2.1.9)$$

Since y_3 is the solution of the equation

$$(\ell^2 + D^2)\, y = 0 \ ,$$

pick y_4 so that it is a solution of the equation

$$(\ell^2 + D^2)y = y_3 \ .$$

Multiplying both sides by $(\ell^2 + D^2)$

$$(\ell^2 + D^2)^2\, y = y_3(\ell^2 + D^2) = 0 \ .$$

So that, y_4 is also a solution of the equation

$$(\ell^2 + D^2)^2\, y = 0 \ .$$

Solve the equation

$$(\ell^2 + D^2)\, y_4 = y_3 \ .$$

Let $y_3 = R_3(r)Z_3(z)$ and $y_4 = R_4(r)Z_4(z)$.

$$(\ell^2 + D^2)R_4Z_4 = R_3Z_3$$

Rearrange

$$\frac{\ell^2 R_4}{R_4} + \frac{D^2 Z_4}{Z_4} = \frac{R_3 Z_3}{R_4 Z_4} \qquad (2.1.10)$$

This is a function of r plus a function of z equal to a product function of r and z. If equation (2.1.10) is to be satisfied identically, the product function must be a function of either r or z only.

(Case i)

Let $Z_4 = aZ_3$, where a = constant.

$$\ell^2 + D^2 = \frac{R_3}{R_4} \cdot \frac{Z_3}{aZ_3}$$

$$R_4 (\ell^2 + D^2) = \frac{1}{a} R_3$$

From equation (2.1.9)

$$(D^2 + k^2) Z_1 = 0$$

and.

$$D^2 = - k^2 .$$

Therefore,

$$R_4(\ell^2 - k^2) = \frac{1}{a} R_3 .$$

Multiply both sides by $(\ell^2 - k^2)$.

$$R_4(\ell^2 - k^2)^2 = \frac{1}{a} R_3(\ell^2 - k^2) = 0$$

Therefore, R, is a solution of

$$(\ell^2 - k^2)^2 R, = 0 .$$

From equation (2.1.4)

$$\ell^2 = \frac{d^2}{dr^2} + \frac{1}{r}\frac{d}{dr} - \frac{1}{r^2}$$

$$\left[\frac{d^2}{dr^2} + \frac{1}{r}\frac{d}{dr} - \left(\frac{1}{r^2} + k^2\right)\right]^2 R_2 = 0$$

The method of solution of this equation is presented in Appendix A.

The solutions of this equation are

$$I_1(kr),\ K_1(kr),\ \frac{d}{dk} I_1(kr),\ \frac{d}{dk} K_1(kr).$$

Since

$$\frac{d}{dk} I_1(kr) = rI_1'(kr) = rI_0(kr) - \frac{1}{k} I_1(kr)$$

and

$$\frac{d}{dk} K_1(kr) = rK_0(kr) - \frac{1}{k} K_1(kr),$$

the four independent integrals are

$$I_1(kr),\ K_1(kr),\ rI_0(kr),\ rK_0(kr).$$

(Case ii)

Let $R_4 = bR_3$.

From equation (2.1.9),

$$(D^2 + k^2)\, Z_1 = 0 \qquad (2.1.11)$$

$$\frac{d^2 Z_1}{dz^2} + k^2 Z_1 = 0$$

$$D^2 = -k^2$$

$$D = \pm ik.$$

Therefore,

$$Z_1 = B_1 \sin kz + B_2 \cos kz \qquad (2.1.11.a)$$

where B_1 and B_2 are constants.

Let $R_4 = bR_3$ in equation (2.1.10) where b equals a constant.

$$(\ell^2 + D^2)Z_4 = Z_3/b$$

From equation (2.1.8)

$$(\ell^2 - k^2)R_1 = 0 \quad \text{or} \quad \ell^2 = k^2.$$

Or, substituting in the above equation

$$(D^2 + k^2)Z_4 = Z_3/b.$$

Multiply both sides by $(D^2 + k^2)$.

$$(D^2 + k^2)^2 Z_4 = \frac{1}{b}(D^2 + k^2)Z_3 = 0$$

Assume the solution

$$Z_4 = A \cos kz.$$

Substitute in the following equation where $\frac{Z_3}{b} = B\cos kz$ from the above solution (2.1.11.a).

$$(D^2 + k^2)Z_4 = B\cos kz$$

Since

$$Z_4 = A\cos kz,$$

$$D^2Z_4 = -k^2A\cos kz,$$

and

$$Z_4(-k^2A\cos kz + k^2A\cos kz) = B\cos kz$$

cannot be solved this way, therefore use the fact that

$$\cos kz = \frac{e^{ikz} + e^{-ikz}}{2}$$

in the equation

$$Z_4 = \frac{1}{D^2 + k^2} \cos kz.$$

$$Z_4 = \frac{1}{D^2 + k^2}\left[\frac{e^{ikz} + e^{-ikz}}{2}\right]$$

$$Z_4 = \frac{1}{D^2 + k^2} \times \frac{e^{ikz}}{2} + \frac{1}{D^2 + k^2} \times \frac{e^{-ikz}}{2}$$

$$Z_4 = \frac{1}{(D+ik)(b-ik)} \times \frac{e^{ikz}}{2} + \frac{1}{(D+ik)(D-ik)} \times \frac{e^{-ikz}}{2}$$

$$Z_4 = \frac{1}{D-ik} \times \frac{e^{ikz}}{4ki} - \frac{1}{D+ik} \times \frac{e^{-ikz}}{4ki}$$

$$Z_4 = \frac{1}{4ki}\left(\frac{eikz}{D-ik} - \frac{e^{-ikz}}{D+ik}\right)$$

$$Z_4 = \frac{1}{4ki}\left[ze^{ikz} - ze^{-ikz}\right]$$

$$Z_4 = \frac{1}{2k} z \sin kz$$

Similarly, it can be shown that

$$Z_4 = \frac{1}{2k} z \cos kz.$$

Therefore, the possible sets of product functions that satisfy $(\ell^2 + D^2)^2 y = 0$ are:

$$
\begin{aligned}
y &= A \cos (kz + \alpha) I_1(kr) \\
y &= B \cos (kz + \beta) K_1(kr) \\
y &= C \cos (kz + \gamma)\, r\, I_0(kr) \\
y &= D \cos (kz + \delta)\, r\, K_0(kr) \\
y &= Ez\cos (kz + \varepsilon) I_1(kr) \\
y &= Fz\cos (kz + \theta) K_1(kr)
\end{aligned}
\qquad (2.1.12)
$$

where $\alpha, \beta, \gamma, \delta, \varepsilon, \theta$ are constants.

Let us consider the general case of the following system of stresses:

(i.) σ_{rr}/μ = a given even fctn of z over the curved surface r = a.

(ii.) σ_{rz}/μ = a given odd fctn of z over the curved surface r = a.

(iii.) $\sigma_{zz} \neq 0$ over the plane ends $z = \pm c$.

Since du/dz and dw/dr are both solutions of $(\ell^2 + D^2)^2 y = 0$ we may express them by a series of terms as follows:

$$
\begin{aligned}
\frac{du}{dz} = \sum \Big\{ & A_1 \cos(kz + \alpha_1) I_1(kr) + C_1 \cos(kz + \gamma_1) r I_0(kr) \\
& + E_1 z \cos(kz + \varepsilon_1) I_1(kr) \Big\}
\end{aligned}
\qquad (2.1.13)
$$

$$
\begin{aligned}
\frac{dw}{dr} = \sum \Big\{ & A_2 \cos(kz + \alpha_2) I_1(kr) + C_2 \cos(kz + y2) r I_0(kr) \\
& + E_2 z \cos(kz + \varepsilon_2) I_1(kr) \Big\} \ .
\end{aligned}
\qquad (2.1.14)
$$

No K-functions have been ihtroduced, as they lead to infinite terms at r = 0.

It can be reasoned that, for a cylinder u should be an even function of z and that w should be an odd function of z (u is symmetric about the z-axis and w is skew-symmetric about the z-axis).

Let

$$\alpha_1 = \alpha_2 = \gamma_1 = \gamma_2 = -\pi/2 \quad ; \quad \varepsilon_1 = \varepsilon_2 = 0$$

The reason for this will be seen upon integration of equations (2.1.13) and (2.1.14) as follows,

$$\frac{du}{dz} = \sum \left\{ A_1 \cos(kz - \pi/2) I_1(kr) + C_1 \cos(kz - \pi/2) r I_0(kr) + E_1 z \cos(kz) I_1(kr) \right\}$$

$$\frac{dw}{dr} = \sum \left\{ A_2 \cos(kz - \pi/2) I_1(kr) + C_2 \cos(kz - \pi/2) r I_0(kr) + E_2 z \cos(kz) I_1(kr) \right\}$$

Expanding the trigonometric functions in equations (2.1.13) and (2.1.14)

$$\frac{du}{dz} = \sum \left\{ A_1 [\cos kz \cos(-\pi/2) + \sin kz \sin(\pi/2)] I_1(kr) + C_1 [\cos kz \cos(-\pi/2) + \sin kz \sin(\pi/2)] r I_0(kr) + E_1 [z \cos(kz) I_1(kr)] \right\}$$

$$\frac{dw}{dr} = \sum \left\{ A_2 [\cos kz \cos(-\pi/2) + \sin kz \sin(\pi/2)] I_1(kr) + C_2 [\cos kz \cos(-\pi/2) + \sin kz \sin(\pi/2)] r I_0(kr) + E_2 z \cos(kz) I_1(kr) \right\}$$

Reducing

$$\frac{dw}{dz} = \sum \left\{ + A_1 \sin(kz) I_1(kr) + C_1 \sin(kz) r I_0(kr) + E_1 z \cos(kz) I_1(kr) \right\}$$

(2.1.15)

$$\frac{dw}{dr} = \sum \left\{ + A_2 \sin(kz) I_1(kr) + C_2 \sin(kz) r I_0(kr) + E_2 z \cos(kz) I_1(kr) \right\}$$

(2.1.16)

Integrating (2.1.15) with respect to z and (2.1.16) with respect to r

$$u = \sum \left\{ - \frac{A_1}{k} \cos(kz) I_1(kr) - \frac{C_1}{k} \cos(kz) r I_0(kr) + \right.$$

$$\left. \frac{E_1}{k} \left(z \sin(kz) + \frac{\cos(kz)}{k} \right) I_1(kr) \right\} + \chi(r) \qquad (2.1.17)$$

$$w = \sum \left\{ \frac{A_2}{k} \sin(kz) I_0(kr) + \frac{C_2}{k} \sin(kz) r I_1(kr) \right.$$

$$\left. + \frac{E_2}{k} z \cos(kz) I_0(kr) \right\} + \theta(z) \qquad (2.1.18)$$

To evaluate the constants, substitute the proper derivatives of (2.1.17) and (2.1.18) into equations (2.1.1) and (2.1.3).

$$(\lambda+2\mu) \left[\sum \left\{ -A_1 k \cos(kz) I_1''(kr) - C_1 k \cos(kz) r I_0''(kr) - \right. \right.$$

$$C_1 \cos(kz) I_0'(kr) - C_1 \cos(kz) I_0'(kr) +$$

$$E_1 \left(z \sin(kz) + \frac{\cos(kz)}{k} \right) k I_1''(kr) + A_1 \cos(kz) \frac{r^{-2}}{k} I_1(kr)$$

$$- A_1 \cos(kz)\, r^{-1} I_1'(kr) - C_1 \cos(kz) I_0'(kr)$$

$$\left. + E_1 \left(z \sin(kz) + \frac{}{k} \left(r^{-1} I_1'(kr) - \frac{r^{-2}}{k} I_1(kr) \right) \right) \right\} + \frac{d^2 \chi(r)}{dr^2}$$

$$+ \frac{1}{r} \frac{d\chi(r)}{dr} - \frac{1}{r^2} \chi(r) \Big] + \mu \left[\sum \left\{ + k A_1 \cos(kz) I_1(kr) \right. \right.$$

$$\left. \left. + k C_1 \cos(kz) r I_0(kr) + E_1 (-k z \sin(kz) + \cos(kz)\, I_1(kr) \right\} \right] +$$

$$+ (\lambda+\mu) \left[\sum \left\{ A_2 \cos(kz) k I_0'(kr) + C_2 \cos(kz)(kr) I_1'(kr) + \right. \right.$$

$$+ C_2\cos(kz)I_1(kr) - E_2 z \sin(kz)kI_0'(kr) +$$

$$E_2\cos(kz)I_0'(kr)\Big\}\Big| \quad = 0 \qquad (2.1.3.a)$$

$$(\lambda+\mu)\Big[\sum\Big\{+ A_1\sin(kz)kI_1'(kr) + C_1\sin(kz)(rk)I_0'(kr)$$

$$+ C_1\sin(kz)I_0(kr) + E_1I_1'(kr)\Big[(kz)\cos(kz)\Big] + \frac{A}{r}\sin(kz)I_1(kr)$$

$$+ C_1\sin(kz)I_0(kr) + \frac{E_1}{r}\left(z\cos(kz)\right)I_1(kr)\Big\}\Big] + \mu\Big[$$

$$\sum\Big\{ kA_2\sin(kz)I_0''(kr) + C_2k\sin(kz)rI_1''(kr) + C_2\sin(kz)I_1'(kr)$$

$$+ C_2\sin(kz)I_1'(kr) + E_2 z\cos(kz)kI_0''(kr) + \frac{A_2}{r}\sin(kz)I_0'(kr)$$

$$+ C_2\sin(kz)I_1'(kr) + \frac{C_2}{rk}\sin(kz)I_1(kr) + \frac{E_2}{r}z\cos(kz)I_0'(kr)\Big\}\Big]$$

$$+ (\lambda+2\mu)\Big[\sum\Big\{-A_2\sin(kz)kI_0(kr) - C_2rk\sin(kz)I_1(kr)$$

$$- E_2 z\cos(kz)kI_0(kr) - E_2\sin(kz)I_0(kr) - E_2\sin(kz)I_0(kr)$$

$$+ \frac{d^2\theta(z)}{dz^2}\Big\}\Big] \quad = 0. \qquad (2.1.3.c)$$

Combine like terms in (2.1.3.a) and (2.1.3.c)

$$(\lambda+2\mu)\Big[\sum\Big\{A_1\cos(kz)\Big(+\frac{r^{-2}}{k}I_1(kr) - kI_1''(kr) - r^{-1}I_1'(kr)\Big)$$

$$- C_1\cos(kz)\Big((kr)I_0''(kr) + 3I_1(kr)\Big) + E_1\Big(z\sin(kz)$$

$$+ \frac{\cos(kz)}{k}\Big)\Big(k\,I_1''(kr) - \frac{r^{-2}}{k}I_1(kr) + r^{-1}I_1'(kr)\Big)\Big\} + \ell^2\chi(r)\Big]$$

$$+ \mu\Big[\sum\Big\{+k\,A_1\cos(kz)I_1(kr) + (rk)\,C_1\cos(kz)I_0(kr)$$

$$+ E_1\Big(-(kz)\sin(kz) + \cos(kz)\Big)I_1(kr)\Big\}\Big] + (\lambda+\mu)\times$$

$$\left[\sum\left\{A_2\cos(kz)kI_1(kr) + C_2\cos(kz)\left((kr)I_1'(kr) + I_1(kr)\right) - E_2\left(z\sin(kz)kI_1(kr) - \cos(kz)I_1(kr)\right)\right\}\right] = 0$$

$$(\lambda+\mu)\left[\sum\left\{+A_1\sin(kz)\left(kI_1'(kr) + r^{-1}I_1(kr)\right) + C_1\sin(kz)\left((kr)I_1(kr) + 2I_0(kr)\right) + E_1\cos(kz)\left((kz)I_1'(kr) + (r^{-1}z)I_1(kr)\right)\right\}\right] + \mu\left[\sum\left\{A_2\sin(kz)\left(kI_1'(kr) + r^{-1}I_1(kr)\right) + C_2\sin(kz)\left((kr)I_1''(kr) + 3I_1'(kr) + (kr)^{-1}I_1(kr)\right) + E_2\cos(kz)\left((kz)I_0''(kr) + (r^{-1}z)\,I_0'(kr)\right)\right\}\right] + (\lambda+2\mu)\left[\sum\left\{-A_2\sin(kz)kI_0(kr) - C_2\sin(kz)(kr)I_1(kr) - E_2\left((kz)\cos(kz)I_0(kr) + 2\sin(kz)I_0(kr)\right)\right\}\right] + D^2\theta(z) = 0$$

In (2.1.3.a) and (2.1.3.c) the recurrence relation $I_0'(kr) = I_1(kr)$ has been used.

It can be shown that we can reduce (2.1.3.a) and (2.1.3.c) to the following four equations.

$$\ell^2\chi(r) = 0 \qquad (2.1.19)$$

$$D^2\theta(z) = 0 \qquad (2.1.20)$$

$$(A_1-A_2)(\lambda+\mu)k^2 + 2k\{C_1(\lambda+2\mu)-\mu E_1 - (\lambda+\mu)E_2\} = 0 \qquad (2.1.21)$$

$$(A_1-A_2)(\lambda+\mu)k^2 + 2k\{C_1(\lambda+\mu) + \mu C_2 - (\lambda+2\mu)E_2\} = 0 \qquad (2.1.22)$$

If we let $C_1 = C_2 = C$ and $E_1 = E_2 = E$, then equations (2.1.21) and (2.1.22) become one equation, as shown

$$(A_1 - A_2)(\lambda+\mu)k^2 + 2k\{C(\lambda+2\mu) - (\lambda+2\mu)E\} = 0$$

or

$$(A_1 - A_2)(\lambda+\mu)k + 2(\lambda+2\mu)(C-E) = 0 . \qquad (2.1.23)$$

By integrating equations (2.1.19) and (2.1.20) we obtain

$$\chi(r) = u_o r \quad \text{and} \quad \theta(z) = w_o z .$$

From equations (2.1.2)

$$\sigma_{rr} = (\lambda+2\mu)\frac{du}{dr} + A\frac{u}{r} + A\frac{dw}{dz}$$

or,

$$\sigma_{rr} = (\lambda+2\mu)\Big[\sum\Big\{-A_1\cos(kz)I_1'(kr) - C\cos(kz)(r)I_0'(kr) - C\cos(kz)(k^{-1})I_0(kr) + E\Big(z\sin(kz) + k^{-1}\cos(kz)\Big)I_1'(kr)\Big\} + d\chi(r)/dr\Big] + \lambda\Big[\sum\Big\{-A_1\cos(kz)(kr)^{-1}I_1(kr) - C\cos(kz)k^{-1}I_0(kr) + E\Big(z\sin(kz) + k^{-1}\cos(kz)\Big)(kr)^{-1}I_1(kr)\Big\} + r^{-1}\chi(r)\Big] + \lambda\Big[\sum\Big\{A_2\cos(kz)I_0(kr) + C\cos(kz)(r)I_1(kr) - E\Big(z\sin(kz)\Big) I_0(kr) - k^{-1}\cos(kz)I_0(kr)\Big\} + d\theta(z)/dz\Big]$$

$$\sigma_{rr} = (2\lambda+2\mu)u_o + A w_o + \sum\Big[-2\mu C\cos(kz)(r)I_1(kr) - 2(\lambda+\mu) C\cos(kz)(k^{-1})I_0(kr) + AEz\sin(kz)I_1'(kr) + AE k^{-1}\cos(kz)I_1'(kr) + 2\mu Ez\sin(kz)I_1'(kr) + 2\mu E k^{-1}\cos(kz)I_1'(kr) + AEz\sin(kz)(kr)^{-1}I_1(kr) + AE k^{-1}\cos(kz)(kr)^{-1}I_1(kr) - AEz\sin(kz)I_0(kr) + AE k^{-1}\cos(kz)I_0(kr) - 2\lambda A_1\cos(kz)I_0(kr) + 2\mu\Big(-A_1\cos(kz)I_1'(kr)\Big) + \lambda A_2\cos(kz)I_0(kr)\Big] .$$

This reduces to

$$\sigma rr = 2(\lambda+\mu)u_o + \lambda\, w_o + \sum\Bigg[-\frac{1}{2}\left\{(2\lambda+3\mu)A_1 + \mu A_2\right\} I_0(kr)\cos kz + 2\mu\left\{\left(A_1 - E/k\right)\frac{I_1(kr)}{kr}\cos kz + Ez\sin kz\left(I_0(kr) - \frac{I_1(kr)}{kr}\right)\right\} - CrI_1(kr)\cos kz\Bigg]. \tag{2.1.24}$$

Likewise,

$$\sigma_{zz} = 2\lambda u_o + (\lambda+2\mu)w_o + \sum\Bigg[\left\{(\lambda+2\mu)A_2 - A\,A_1 - \lambda\,\frac{2C}{k}\right. + 2(\lambda+\mu)\, I_0(kr)\cos kz + 2\mu\left\{CrI_1(kr)\cos kz - E\,I_0(kr)z\,\sin kz\right\}\Bigg] \tag{2.1.25}$$

and

$$\sigma_{rz} = \mu\sum\left\{(A_1 + A_2)I_1(kr)\sin kz + 2CrI_0(kr)\sin kz + 2EI_1(kr)z\,\cos kz\right\}. \tag{2.1.26}$$

For the displacements let $E_1 = E_2 = 0$ and $C_1 = C_2 = C$ and substitute $\chi(r) = u_o r$ and $\theta(z) = w_o z$ into equations (2.1.17) and (2.1.18). Then with $kr = \rho$

$$u = u_o r + \sum\left\{-\frac{A_1}{k} I_1(\rho) - \frac{C}{k} rI_0(\rho)\right\}\cos kz \tag{2.1.17,a}$$

$$w = w_o z + \sum\left\{\frac{A_2}{k} I_0(\rho) + \frac{C}{k} rI_1(\rho)\right\}\sin kz. \tag{2.1.18,a}$$

Let us consider our cylinder so that the coordinate system may be defined and that the boundary conditions may be established. The coordinate system is as defined in Figure 1.

The boundary conditions are as follows:

(i) A total pressure $\pi a^2 Q$ exists over the plane ends, the distribution of this pressure being, however, unknown.

(ii) w = constant when $z = \pm c$.

(iii) $u = 0$ when $r = a$, $z = \pm c$.

(iv) $\sigma_{rr} = 0$ when $r = a$,

$\sigma_{rz} = 0$ when $r = a$.

Filon has shown that a solution of the form shown in equation (2.1.17.a) and (2.1.18.a) plus a finite power series in r and z will satisfy the boundary conditions, incompressibility condition, and equilibrium equations which have been specified. This assumed solution is given below.

$$u = \sum \left\{ -\frac{A_1}{k} I_1(kr) - \frac{C}{k} r I_0(kr) \right\} \cos kz + u_0 r + \frac{u_1 r^3}{3} + \frac{Drz^2}{2} + \frac{Er^3 z^2}{2} + \frac{Frz^4}{4} \qquad (2.1.27)$$

and

$$w = \sum \left\{ \frac{A_2}{k} I_0(kr) + \frac{C}{k} r I_1(kr) \right\} \sin kz + w_0 z + \frac{w_1 z^3}{3} + \frac{w_2 z^5}{5} + \frac{D^1 r^2 z}{2} + \frac{E^1 r^2 z^3}{2} - \frac{F^1 r^4 z}{4} \qquad (2.1.28)$$

These sums of series have been restricted by the conditions that u must be odd in r and even in z, and that w must be even in r and odd in z.

The method of solving for the unknown constants, that was employed by Filon, cannot be used in the problem that is ultimately considered here. Filon was dealing with linear equations and the

equations to be considered here are non-linear because this study involves a rubber-like material which has the characteristic of large deformations. For this reason Filon's method of solution will not be given here because it would not contribute anything toward a better understanding of the problem, Instead, the constants of equations (2.1.27) and (2.1.28), as found by Filon, will be presented.

$$
\begin{aligned}
u_o &= \frac{Qg(2\gamma-1)}{\mu[h + (2\gamma-1)f + 2g(4\gamma-1)]} \\
u_1 &= \frac{3}{8}\left[(1-\gamma)a^2 - \frac{4}{3}c^2\right]E \\
u_2 &= -\frac{5}{24}(1-\gamma)E \\
D &= \left\{\frac{4}{3}(1-\gamma)c^2 - a^2\right\}E \\
E &= \frac{-Q(2\gamma-1)}{p[h + (2\gamma-1)f + 2g(4\gamma-1)]} \\
F &= -\frac{4}{3}(1+\gamma)E \\
w_o &= -\frac{Qh(1-\gamma) + 2g\gamma}{\mu[h + (2\gamma-1)f + 2g(4\gamma-1)]} \\
w_1 &= \left[a^2 - \frac{8c^2}{3}\right]\gamma E \\
w_2 &= \frac{4}{3}\gamma E \\
D^1 &= \frac{4\gamma c^2}{3}E \\
E^1 &= -\frac{4}{3}\gamma E \\
F^1 &= 0
\end{aligned}
\qquad (2.1.29)
$$

$$k = \frac{n\pi}{c} , \quad n=1,2,3,\ldots \tag{2.1.30}$$

where

$$f = (2\gamma-1)\frac{a^4}{6} + \frac{1}{3}a^2c^2 - \frac{1}{5}(2\gamma+1)c^4$$

$$g = \frac{1}{12}(1-\gamma-\zeta)a^4 - \frac{1}{6}a^2c^2 + \frac{1}{3}\left[1+\gamma - \frac{4}{15}[2\gamma+1]\right]c^4$$

$$h = -\frac{14}{15}c^4\gamma - \frac{a^4}{12}(2\gamma+1) + \frac{2a^2c^2\gamma}{3} \tag{2.1.31}$$

$$\zeta = \sum_1^\infty \frac{24}{\alpha^3}\frac{[(2\gamma+1)\alpha + \frac{4}{\alpha}(8\gamma+1)]I_1^2 - (8\gamma+4)I_0I_1}{\gamma\alpha^2I_0^2 - I_1^2(1+\gamma\alpha^2)}$$

$$\gamma = \frac{\lambda+\mu}{\lambda+2\mu}$$

$$\alpha = ka = \frac{n\pi a}{c}$$

In the above,

$$\zeta = \sum_1^\infty \frac{24}{\alpha^3}\frac{[(2\gamma+1)\alpha + \frac{4}{\alpha}(8\gamma+1)]I_1^2 - (8\gamma+4)I_1I_0}{\gamma\alpha^2I_0^2 - I_1^2(1+\gamma\alpha^2)} . \tag{2.1.32}$$

We also have,

$$C_n = \frac{(-1)^{n+1}}{2}\frac{\gamma E 4a^2}{kI_1}\frac{\left[(2\gamma+1)\alpha + \frac{4(8\gamma+1)}{\alpha}\right]I_1^2 - 4I_0I_1(2\gamma+1)}{\gamma\alpha^2I_0^2 - (1+\gamma\alpha^2)I_1^2} , \tag{2.1.33}$$

$$A_{2n} = \frac{(-1)^n}{2}\frac{16ac^3}{n^3\pi^3}(2\gamma+1)E + C_n\left[\frac{\zeta}{\gamma k} - \frac{2aI_0}{I_1}\right] \tag{2.1.34}$$

and

$$A_{1n} = A_{2n} - 1.53\frac{C_n}{n} . \tag{2.1.35}$$

2.2 Review of Finite Deformation Theory

The basic equations of the finite deformation theory were derived by E. and F. Cosserat in 1896. The following equations were set forth by Rivlin *(6)* in 1948. They are set **forth** here as a foundation upon which the theoretical portion of this present work rests. Rivlin has introduced the concept of a neo-Hookean material. This material is assumed to be incompressible and isotropic in its undeformed state and is capable of large, elastic deformations. Rivlin has defined the stress-strain relationships **for** this neo-Hookean material **and** using these relationships has developed a mathematical theory for the material. The principal results obtained have been expressed with reference to a cylindrical polar coordinate system (r,θ,z) and have been set forth in the following.

The strain components are defined as being at the point which is at (r,θ,z) in the undeformed state, as shown in Figure 1.

$$
\begin{aligned}
1 + 2\varepsilon_{rr} &= \left(1 + \frac{\partial u}{\partial r}\right)^2 + \left(\frac{\partial v}{\partial r}\right)^2 + \left(\frac{\partial w}{\partial r}\right)^2 , \\
1 + 2\varepsilon_{\theta\theta} &= \frac{1}{r^2}\left(\frac{\partial u}{\partial \theta} - v\right)^2 + \left(1 + \frac{u}{r} + \frac{1}{r}\frac{\partial v}{\partial \theta}\right)^2 + \frac{1}{r^2}\left(\frac{\partial w}{\partial \theta}\right)^2 , \\
1 + 2\varepsilon_{zz} &= \left(\frac{\partial u}{\partial z}\right)^2 + \left(\frac{\partial v}{\partial z}\right)^2 + \left(1 + \frac{\partial w}{\partial z}\right)^2 , \\
\varepsilon_{\theta z} &= \frac{1}{r}\left(\frac{\partial u}{\partial \theta} - v\right)\frac{\partial u}{\partial z} + \left(1 + \frac{u}{r} + \frac{1}{r}\frac{\partial v}{\partial \theta}\right)\frac{\partial v}{\partial z} + \frac{1}{r}\frac{\partial w}{\partial \theta}\left(1 + \frac{\partial w}{\partial z}\right) , \\
\varepsilon_{zr} &= \frac{\partial u}{\partial z}\left(1 + \frac{\partial u}{\partial r}\right) + \frac{\partial v}{\partial z}\frac{\partial v}{\partial r} + \left(1 + \frac{\partial w}{\partial z}\right)\frac{\partial w}{\partial r} , \\
\varepsilon_{r\theta} &= \left(1 + \frac{\partial u}{\partial r}\right)\frac{1}{r}\left(\frac{\partial u}{\partial \theta} - v\right) + \frac{\partial v}{\partial r}\left(1 + \frac{u}{r} + \frac{1}{r}\frac{\partial v}{\partial \theta}\right) + \frac{\partial w}{\partial r}\frac{1}{r}\frac{\partial w}{\partial \theta} .
\end{aligned}
\tag{2.2.1}
$$

The incompressibility condition, using a cylindrical polar coordinate system, is

$$\tau = \begin{vmatrix} 1 + \frac{\partial u}{\partial r} & \frac{1}{r}\left(\frac{\partial v}{\partial \theta} - v\right) & \frac{\partial u}{\partial z} \\ \frac{\partial v}{\partial r} & 1 + \frac{u}{r} + \frac{1}{r}\frac{\partial v}{\partial \theta} & \frac{\partial v}{\partial z} \\ \frac{\partial w}{\partial r} & \frac{1}{r}\frac{\partial w}{\partial \theta} & 1 + \frac{\partial w}{\partial z} \end{vmatrix} = 1. \qquad (2.2.2)$$

Since, in the deformation, the point (r,θ,z) moves to $(r+s, \theta+\phi, z+w)$,

$$u = (r+s)\cos\phi - r, \text{ and } v = (r+s)\sin\phi. \qquad (2.2.3)$$

Therefore, it has been shown that the stresses in terms of displacements can be written as,

$$\begin{aligned}
\sigma_{rr} &= \frac{1}{3}E\left[\left(1 + \frac{\partial s}{\partial r}\right)^2 + \frac{1}{r^2}\left(\frac{\partial s}{\partial \theta}\right)^2 + \left(\frac{\partial s}{\partial z}\right)^2\right] + p, \\
\sigma_{\theta\theta} &= \frac{1}{3}E\,(r+s)^2\left[\left(\frac{\partial \phi}{\partial r}\right)^2 + \frac{1}{r^2}\left(1 + \frac{\partial \phi}{\partial \theta}\right)^2 + \left(\frac{\partial \phi}{\partial z}\right)^2\right] + p, \\
\sigma_{zz} &= \frac{1}{3}E\left[\left(\frac{\partial w}{\partial r}\right)^2 + \frac{1}{r^2}\left(\frac{\partial w}{\partial \theta}\right)^2 + \left(1 + \frac{\partial w}{\partial z}\right)^2\right] + p, \\
\sigma_{\theta z} &= \frac{1}{3}E\,(r+s)\left[\frac{\partial \phi}{\partial r}\frac{\partial w}{\partial r} + \frac{1}{r^2}\frac{\partial w}{\partial \theta}\left(1 + \frac{\partial \phi}{\partial \theta}\right) + \left(1 + \frac{\partial w}{\partial z}\right)\frac{\partial \phi}{\partial z}\right], \\
\sigma_{zr} &= \frac{1}{3}E\left[\frac{\partial w}{\partial r}\left(1 + \frac{\partial s}{\partial r}\right) + \frac{1}{r^2}\frac{\partial w}{\partial \theta}\frac{\partial s}{\partial \theta} + \left(1 + \frac{\partial w}{\partial z}\right)\frac{\partial s}{\partial z}\right], \\
\sigma_{r\theta} &= \frac{1}{3}E(r+s)\left[\left(1 + \frac{\partial s}{\partial r}\right)\frac{\partial \phi}{\partial r} + \frac{1}{r^2}\frac{\partial s}{\partial \theta}\left(1 + \frac{\partial \phi}{\partial \theta}\right) + \frac{\partial s}{\partial z}\frac{\partial \phi}{\partial z}\right].
\end{aligned} \qquad (2.2.4)$$

The equations of motion are

$$\alpha = \left[\left(1 + \frac{u}{r} + \frac{1}{r}\frac{\partial v}{\partial \theta}\right)\left(1 + \frac{\partial w}{\partial z}\right) - \frac{1}{r}\frac{\partial w}{\partial \theta}\frac{\partial v}{\partial z}\right]\frac{\partial p}{\partial r} + \left[\frac{\partial v}{\partial z}\frac{\partial w}{\partial r} - \frac{\partial v}{\partial r}\left(1 + \frac{\partial w}{\partial z}\right)\right]\frac{1}{r}\frac{\partial p}{\partial \theta} +$$

$$+ \left[\frac{1}{r}\frac{\partial w}{\partial \theta}\frac{\partial v}{\partial r} - \frac{\partial w}{\partial r}\left(1 + \frac{u}{r} + \frac{1}{r}\frac{\partial v}{\partial \theta}\right)\right]\frac{\partial p}{\partial z}$$

$$\beta = \left[\frac{1}{r}\frac{\partial w}{\partial \theta}\frac{\partial u}{\partial z} - \frac{1}{r}\left(\frac{\partial u}{\partial \theta} - v\right)\left(1 + \frac{\partial w}{\partial z}\right)\right]\frac{\partial p}{\partial r} + \left[\left(1 + \frac{\partial u}{\partial r}\right)\left(1 + \frac{\partial w}{\partial z}\right) - \frac{\partial u}{\partial z}\frac{\partial w}{\partial r}\right]\frac{1}{r}\frac{\partial p}{\partial \theta} +$$

$$+ \left[\frac{1}{r}\left(\frac{\partial u}{\partial \theta} - v\right)\frac{\partial w}{\partial r} - \frac{1}{r}\frac{\partial w}{\partial \theta}\left(1 + \frac{\partial u}{\partial r}\right)\right]\frac{\partial p}{\partial z}.$$

and

$$\gamma = \left[\frac{1}{r}\left(\frac{\partial u}{\partial \theta} - v\right)\frac{\partial v}{\partial z} - \left(1 + \frac{u}{r} + \frac{1}{r}\frac{\partial v}{\partial \theta}\right)\frac{\partial u}{\partial z}\right]\frac{\partial p}{\partial r} + \left[\frac{\partial u}{\partial z}\frac{\partial v}{\partial r} - \left(1 + \frac{\partial u}{\partial r}\right)\frac{\partial v}{\partial z}\right]\frac{1}{r}\frac{\partial p}{\partial \theta} +$$

$$+ \left[\left(1 + \frac{\partial u}{\partial r}\right)\left(1 + \frac{u}{r} + \frac{1}{r}\frac{\partial v}{\partial \theta}\right) - \frac{1}{r}\frac{\partial v}{\partial r}\left(\frac{\partial u}{\partial \theta} - v\right)\right]\frac{\partial p}{\partial z}$$

where (2.2.5)

$$\alpha = \rho_o \frac{\partial^2 u}{\partial t^2} - \rho_o R_1 - \frac{1}{3}E\left(\frac{\partial^2 u}{\partial r^2} + \frac{1}{r}\frac{\partial u}{\partial r} + \frac{1}{r}\frac{\partial^2 u}{\partial \theta^2} + \frac{2}{r^2}\frac{\partial v}{\partial \theta} - \frac{u}{r^2} + \frac{\partial^2 u}{\partial z^2}\right),$$

$$\beta = \rho_o \frac{\partial^2 v}{\partial t^2} - \rho_o \Theta - \frac{1}{3}E\left(\frac{\partial^2 v}{\partial r^2} + \frac{1}{r}\frac{\partial v}{\partial r} + \frac{1}{r^2}\frac{\partial^2 v}{\partial \theta^2} + \frac{2}{r^2}\frac{\partial u}{\partial \theta} - \frac{v}{r^2} + \frac{\partial^2 v}{\partial z^2}\right),$$

$$\gamma = \rho_o \frac{\partial^2 w}{\partial t^2} - \rho_o Z_1 - \frac{1}{3}E\left(\frac{\partial^2 w}{\partial r^2} + \frac{1}{r}\frac{\partial w}{\partial r} + \frac{1}{r^2}\frac{\partial^2 w}{\partial \theta^2} + \frac{\partial^2 w}{\partial z^2}\right).$$

(2.2.6)

In the equations of motion, ρ_o is the density of the material and R_1, Θ, and Z_1 are the componehts of ***any*** **body** forces on the material in the r,θ, and z directions respectively.

If the surface of the **body** considered has, in the undeformed state, the shape of a cylinder with the z-axis as the axis of symmetry,

the boundary conditions will be different on the plane and curved surfaces. Rivlin has shown the boundary conditions to be, for the curved and plane surfaces respectively,

$$\frac{1}{3}E\left(1 + \frac{u}{r}\right) - R_\nu = -p\left[\left(1 + \frac{u}{r} + \frac{1}{r}\frac{\partial v}{\partial \theta}\right)\left(1 + \frac{\partial w}{\partial z}\right) - \frac{1}{r}\frac{\partial w}{\partial \theta}\frac{\partial v}{\partial z}\right],$$

$$\frac{1}{3}E\frac{\partial v}{\partial r} - \Theta_\nu = -p\left[\frac{1}{r}\frac{\partial w}{\partial \theta}\frac{\partial u}{\partial z} - \frac{1}{r}\left(\frac{\partial u}{\partial \theta} - v\right)\left(1 + \frac{\partial w}{\partial z}\right)\right], \qquad (2.2.7)$$

$$\frac{1}{3}E\frac{\partial w}{\partial r} - Z_\nu = -p\left[\frac{1}{r}\left(\frac{\partial u}{\partial \theta} - v\right)\frac{\partial v}{\partial z} - \left(1 + \frac{u}{r} + \frac{1}{r}\frac{\partial v}{\partial \theta}\right)\frac{\partial u}{\partial z}\right].$$

and

$$\frac{1}{3}E\frac{\partial u}{\partial z} - R_\nu = -p\left[\frac{1}{r}\frac{\partial w}{\partial \theta}\frac{\partial v}{\partial r} - \frac{\partial w}{\partial r}\left(1 + \frac{u}{r} + \frac{1}{r}\frac{\partial v}{\partial \theta}\right)\right],$$

$$\frac{1}{3}E\frac{\partial v}{\partial z} - \Theta_\nu = -p\left[\frac{1}{r}\left(\frac{\partial u}{\partial \theta} - v\right)\frac{\partial w}{\partial r} - \frac{1}{r}\frac{\partial w}{\partial \theta}\left(1 + \frac{\partial u}{\partial r}\right)\right], \qquad (2.2.8)$$

$$\frac{1}{3}E\left(1 + \frac{\partial w}{\partial z}\right) - Z_\nu = -p\left[\left(1 + \frac{\partial u}{\partial r}\right)\left(1 + \frac{u}{r} + \frac{1}{r}\frac{\partial v}{\partial \theta}\right) - \frac{1}{r}\left(\frac{\partial u}{\partial \theta} - v\right)\frac{\partial v}{\partial r}\right].$$

These equations can be simplified greatly, viz. If, as in the problem considered here, the deformation possesses cylindrical symmetry about the z-axis!, then u,v,w, and p are independent of θ, i.e.,

$$\frac{\partial u}{\partial \theta} = \frac{\partial v}{\partial \theta} = \frac{\partial w}{\partial \theta} = \frac{\partial p}{\partial \theta} = 0 .$$

Introducing this into equation (2.2.1) for the strains and with the equation $v = 0$ for all points (r,θ,z) because no rotation about the z-axis occurs,

$$
\begin{aligned}
1 + 2\varepsilon_{rr} &= \left(1 + \frac{\partial u}{\partial r}\right)^2 + \left(\frac{\partial w}{\partial r}\right)^2 , \\
1 + 2\varepsilon_{\theta\theta} &= \left(1 + \frac{u}{r}\right)^2 , \\
1 + 2\varepsilon_{zz} &= \left(\frac{\partial u}{\partial z}\right)^2 + \left(1 + \frac{\partial w}{\partial z}\right)^2 , \\
\varepsilon_{\theta z} &= 0 , \\
\varepsilon_{zr} &= \frac{\partial u}{\partial z}\left(1 + \frac{\partial u}{\partial r}\right) + \left(1 + \frac{\partial w}{\partial z}\right)\frac{\partial w}{\partial r} , \\
\varepsilon_{re} &= 0 .
\end{aligned}
\tag{2.2.9}
$$

The incompressibility condition becomes,

$$
\tau = \begin{vmatrix} 1 + \dfrac{\partial u}{\partial r} & 0 & \dfrac{\partial u}{\partial z} \\ 0 & 1 + \dfrac{u}{r} & 0 \\ \dfrac{\partial w}{\partial r} & 0 & 1 + \dfrac{\partial w}{\partial z} \end{vmatrix} \tag{2.2.10}
$$

The **equations of equilibrium become, with R, = Θ = Z$_1$ = 0 and**

$$
\frac{\partial^2 u}{\partial t^2} = \frac{\partial^2 v}{\partial t^2} = \frac{\partial^2 w}{\partial t^2} = 0 ,
$$

$$
-\frac{1}{3}E\left(\frac{\partial^2 u}{\partial r^2} + \frac{1}{r}\frac{\partial u}{\partial r} - \frac{u}{r^2} + \frac{\partial^2 u}{\partial z^2}\right) = \left(1 + \frac{u}{r}\right)\left(1 + \frac{\partial w}{\partial z}\right)\frac{\partial p}{\partial r} - \frac{\partial w}{\partial r}\left(1 + \frac{u}{r}\right)\frac{\partial p}{\partial z} ,
\tag{2.2.11}
$$

and

$$
-\frac{1}{3}E\left(\frac{\partial^2 w}{\partial r^2} + \frac{1}{r}\frac{\partial w}{\partial r} + \frac{\partial^2 w}{\partial z^2}\right) = -\left(1 + \frac{u}{r}\right)\frac{\partial u}{\partial z}\frac{\partial p}{\partial r} + \left(1 + \frac{\partial u}{\partial r}\right)\left(1 + \frac{u}{r}\right)\frac{\partial p}{\partial z} .
\tag{2.2.12}
$$

The boundary conditions become, for the surface parallel to the z-axis and cylindrical in shape,

$$\frac{1}{3} E \left(1 + \frac{\partial u}{\partial r}\right) = - p\left(1 + \frac{u}{r}\right)\left(1 + \frac{\partial w}{\partial z}\right) \tag{2.2.13}$$

and

$$\frac{1}{3} \frac{\partial w}{\partial r} = -p\left[- \left(1 + \frac{u}{r}\right) \frac{\partial u}{\partial z}\right] , \tag{2.2.14}$$

and for the plane surfaces which are normal to the z-axis,

$$\frac{1}{3} E \frac{\partial u}{\partial z} - R_{\nu} = - p\left[- \frac{\partial w}{\partial r} \left(1 + \frac{u}{r}\right)\right] \tag{2.2.15}$$

and

$$\frac{1}{3} E\left(1 + \frac{\partial w}{\partial z}\right) - Z_{\nu} = -p\left[\left(1 + \frac{\partial u}{\partial r}\right)\left(1 + \frac{u}{r}\right)\right]. \tag{2.2.16}$$

For the curved surface R_{ν} and Z_{ν} have been taken as zero because for this specific problem that is the case.

2.3 Finite Deformation Theory Applied to the Problem

In the previous section the equations describing the stresses, strains, etc. of a right circular cylinder under an arbitrary system of loads have been presented. In this section an attempt to solve these equations for prescribed boundary conditions and a prescribed system of loading has been attempted. The body considered, along with the coordinate system used in the solution, is shown in Figure 1. In this derivation $2c = L$.

The displacement boundary conditions are

(i.) $w\left(r, \frac{L}{2}\right) = K = \text{constant}$,

(ii.) $u(o,z) = 0$,

and

(iii.) $u\left(a,\frac{L}{2}\right) = 0.$

The third condition states that there is no displacement in the radial direction at the edges (r=a) of the ends of the cylinder.

The stress boundary conditions are

(i.) no stresses exist on the curved surface,

(ii.) a shear stress due to friction exists on each of the plane surfaces,

and

(iii.) a normal compressive stress, with unknown distribution with respect to r, exists on each of the plane surfaces.

Proceding from Filon's solution of displacements, the solution, in terms of displacements, will be assumed to be some general function of r times a sine or cosine series in z plus a finite power series in r and z. It must also be assumed that u is odd in r and even in z and that w is even in r and odd in z. The assumed solutions are then

$$u = f(r)\ \text{coskz} + \sum_{0}^{w}\sum_{0}^{\infty} A_{mn} r^{2n+1} z^{2m}$$

and

$$w = g(r)\ \text{sinkz} + \sum_{0}^{\infty}\sum_{0}^{m} B_{mn} r^{2n} z^{2m+1}$$

where f(r) must be odd in r and g(r) must be even in r.

Apply the displacement boundary Conditions as follows:

(i.) $$w\left(r,\frac{L}{2}\right) = K = g(r)\ \sin k\,\frac{L}{2} + \sum_{0}^{\infty}\sum_{0}^{\infty} B_{mn} r^{2n}\left[\frac{L}{2}\right]^{2m+1}$$

$$\sin k\,\frac{L}{2} \equiv 0$$

$$k\frac{L}{2} = mv \qquad \text{for } m = 1,2,3,\ldots$$

$$\underline{k = \frac{2m\pi}{L}} \tag{2.3.1}$$

also

$$\sum_{0}^{m}\sum_{n=1}^{m} B_{mn} r^{2n}\left(\frac{L}{2}\right)^{2m+1} = 0 \tag{2.3.2}$$

(ii.) $$u(o,z) = 0 = f(o)\cos kz + \sum_{0}^{m}\sum_{0}^{m} A_{mn}(o)z^{2m}$$

$$\underline{f(o) = 0} \tag{2.3.3}$$

(iii.) $$u\left(a,\frac{L}{2}\right) = 0 = \sum_{0}^{\infty} f(a)\cos(m\pi) + \sum_{0}^{\infty}\sum_{0}^{\infty} A_{mn}a^{2n+1}\left(\frac{L}{2}\right)^{2m}$$

$$\underline{\sum_{0}^{\infty}(-1)^{m}f(a) + \sum_{0}^{\infty}\sum_{0}^{\infty} A_{mn}a^{2n+1}\left(\frac{L}{2}\right)^{2m} = 0} \tag{2.3.4}$$

Referring to equations (2.2.13) through (2.2.16), apply the stress boundary conditions for the cylindrical surface where r=a and z=z,

$$\frac{1}{3}E\left[1 + \sum_{0}^{m} f'(a)\cos\frac{2m\pi z}{L} + \sum_{0}^{m}\sum_{0}^{m} A_{mn}(2n+1)a^{2n}z^{2m}\right] = -p(a,z)$$

$$\left[1 + \sum_{0}^{\infty}\frac{f(a)}{a}\cos\frac{2m\pi z}{L} + \sum_{0}^{\infty}\sum_{0}^{\infty} A_{mn}a^{2n}z^{2m}\right]\left[1 + \sum_{0}^{m} g(a)\frac{2m\pi}{L}\cos\frac{2m\pi z}{L} + \right.$$

$$\left. + \sum_{0}^{m}\sum_{0}^{m} B_{mn}(2m+1)a^{2n}z^{2m}\right] \tag{2.3.5}$$

and

$$\frac{1}{3}E\left[\sum_{0}^{\infty} g'(a)\sin\frac{2m\pi z}{L} + \sum_{0}^{\infty}\sum_{0}^{\infty} B_{mn}2n\,a^{2n-1}z^{2m+1}\right] = +p(a,z)\times$$

$$\left[1 + \sum_{0}^{\infty} \frac{f(a)}{a} \cos\frac{2m\pi z}{L} - \sum_{0}^{m}\sum_{0}^{m} A_{mn} a^{2n} z^{2m}\right]\left[-\int_{0}^{m} f(a)\,\% \sin\frac{2m\pi z}{1} -\right.$$

$$\left.\sum_{0}^{m}\sum_{0}^{m} A_{mn}\, 2m\, a^{2n+1} z^{2m-1}\right], \qquad (2.36)$$

and for the plane surface where $r = r$ and $z = L/2$,

$$\frac{1}{3} E\left[-\sum_{0}^{m} f(r)\,\frac{2m\pi}{L}\,\sin(m\pi) + \sum_{0}^{\infty}\sum_{0}^{\infty} A_{mn}\, 2m\, r^{2n+1}\left(\frac{L}{2}\right)^{2m-1}\right] - RV =$$

$$= + p\left(r,\frac{L}{2}\right)\left[1 + \sum_{0}^{\infty}\frac{f(r)}{r}\cos(m\pi) + \sum_{0}^{\infty}\sum_{0}^{\infty} A_{mn} r^{2n}\left(\frac{L}{2}\right)^{2m}\right]\left[\sum_{0}^{\infty} g'(r)\sin(m\pi) +\right.$$

$$\left. + \sum_{0}^{m}\sum_{0}^{\infty} B_{mn}\, 2n\, r^{2n-1}\left(\frac{L}{2}\right)^{2m+1}\right]$$

and

$$\frac{1}{3} E\left[1 + \sum_{0}^{m} g(r)\,\frac{2m\pi}{L}\cos(m\pi) + \sum_{0}^{m}\sum_{0}^{m} B_{mn}(2m+1) r^{2n}\left(\frac{L}{2}\right)^{2m}\right] = -p\left(r,\frac{L}{2}\right)\times$$

$$\left[1 + \sum_{0}^{m} f'(r)\cos(m\pi) + \sum_{0}^{m}\sum_{0}^{m} A_{mn}(2n+1) r^{2n}\left(\frac{L}{2}\right)^{2m}\right]\left[1 + \sum_{0}^{\infty}\frac{f(r)}{r}\cos(m\pi) +\right.$$

$$\left. + \sum_{0}^{\infty}\sum_{0}^{\infty} A_{mn} r^{2n}\left(\frac{L}{2}\right)^{2m}\right] + Z_{\nu}$$

These equations reduce to

$$\frac{1}{3} E\left[\sum_{0}^{m}\sum_{0}^{m} A_{mn}\, 2m\, r^{2n+1}\left(\frac{L}{2}\right)^{2q-1}\right] - R_{\nu} = p\left(r,\frac{L}{2}\right)\left[1 + \sum_{0}^{\infty}\frac{f(r)}{r}(-1)^{m} +\right.$$

$$\left. + \sum_{0}^{\infty}\sum_{0}^{\infty} A_{mn} r^{2n}\left(\frac{L}{2}\right)^{2m}\right]\left[\sum_{0}^{m}\sum_{0}^{m} B_{mn}\, 2n\, r^{2n-1}\left(\frac{L}{2}\right)^{2m+1}\right], \qquad (2.3.7)$$

and

$$\frac{1}{3} E\left[1 + \sum_{0}^{m} g(r)\,\frac{2m\pi}{L}(-1)^{m} + \sum_{0}^{m}\sum_{0}^{m} Bmn(2m+1) r^{2n}\left(\frac{L}{2}\right)^{2m}\right] = -p\left(r,\frac{L}{2}\right)$$

$$\left[1 + \sum_{0}^{m} f'(r)(-1)^{m} + \sum_{0}^{m}\sum_{0}^{m} A_{mn}(2n+1) r^{2n}\left(\frac{L}{2}\right)^{2m}\right]\left[1 + \sum_{0}^{\infty}\frac{f(r)}{r}(-1)^{m} +\right.$$

$$+ \sum_{o}^{\infty}\sum_{o}^{\infty} A_{mn}\, r^{2n}\left(\frac{L}{2}\right)^{2m}\Bigg] + Z_{\nu} \,. \qquad (2.3.8)$$

Letting r go to a in equations (2.3.7), and (2.3.8),

$$\frac{1}{3} E\left[\sum_{o}^{\infty}\sum_{o}^{\infty} A_{mn}\, 2m\, a^{2n+1}\left(\frac{L}{2}\right)^{2m-1}\right] = p\left(a,\frac{L}{2}\right)\left[1 + \sum_{o}^{\infty}\frac{f(a)}{a}(-1)^{m} + \right.$$

$$\left. + \sum_{o}^{m}\sum_{o}^{m} A_{mn} a^{2n}\left(\frac{L}{2}\right)^{2m}\right]\left[\sum_{o}^{\infty}\sum_{o}^{\infty} B_{mn}\, 2n\, a^{2n-1}\left(\frac{L}{2}\right)^{2m+1}\right]$$

$$\frac{1}{3} E\left[1 + \sum_{o} g(a)\,\frac{2m\pi}{L}(-1)^{m} + \sum_{o}^{m}\sum_{o}^{m} B_{mn}(2m+1)a^{2n}\left(\frac{L}{2}\right)^{2m}\right] = - p\left(a,\frac{L}{2}\right)$$

$$\left[1 + \sum_{o}^{m} f'(a)(-1)^{m} + \sum_{o}^{m}\sum_{o}^{m} A_{mn}(2n+1)a^{2n}\left(\frac{L}{2}\right)^{2m}\right]\left[1 + \sum_{o}^{m}\frac{f(a)}{a}(-1)^{m} + \right.$$

$$\left. + \sum_{o}^{\infty}\sum_{o}^{\infty} A_{mn} a^{2n}\left(\frac{L}{2}\right)^{2m}\right] .$$

Eliminating $p\left(a,\frac{L}{2}\right)$

$$\left[1 + \sum_{o}^{\infty} g(a)\,\frac{2m\pi}{L}(-1)^{m} + \sum_{o}^{\infty}\sum_{o}^{\infty} B_{mn}(2m+1)a^{2n}\left(\frac{L}{2}\right)^{2m}\right]\left[\sum_{o}^{\infty}\sum_{o}^{\infty} B_{mn}\, 2na^{2n-1}\left(\frac{L}{2}\right)^{2m+1}\right] =$$

$$\left[\sum_{o}^{\infty}\sum_{o}^{\infty} A_{mn}\, 2m\, a^{2n+1}\left(\frac{L}{2}\right)^{2m-1}\right]\left[1 + \sum_{o}^{\infty} f'(a)(-1)^{m} + \sum_{o}^{\infty}\sum_{o}^{\infty} A_{mn}(2n+1)a^{2n}\left(\frac{L}{2}\right)^{2m}\right] . \qquad (2.3.9)$$

Equation (2.3.9) is the condition at r = a and z = L/2. If in equations (2.3.5) and (2.3.6), $z \to L/2$ the same equation results, therefore, the boundary conditions match at r = a and z = L/2.

Consider equation (2.3.2),

$$\sum_{o}^{\infty}\sum_{n=1}^{\infty} B_{mn} r^{2n}\left(\frac{L}{2}\right)^{2m+1} = 0 \,.$$

Differentiating equation (2.3.2) with respect to r,

$$\frac{\partial}{\partial r}\left[\sum_{o}^{\infty}\sum_{n=1}^{\infty} B_{mn}\, r^{2n}\left(\frac{L}{2}\right)^{2m+1}\right] = \sum_{o}^{\infty}\sum_{n=1}^{\infty} B_{mn}\, 2nr^{2n-1}\left(\frac{L}{2}\right)^{2m+1} = 0 .$$

Substituting this into equation (2.3.7)

$$\frac{1}{3} E\left[\sum_{o}^{\infty}\sum_{o} A_{mn}\, 2mr2n+1\left(\frac{L}{2}\right)2m-1\right] - R_{\nu} = p\left(r,\frac{L}{2}\right)\left[1 + \sum_{o}^{\infty}\frac{f(r)}{r}(-1)^{m} + \right.$$

$$\left. + \sum_{o}^{m}\sum_{o}^{m} A_{mn}\, r^{2n}\left(\frac{L}{2}\right)^{2m}\right]\left[0\right]$$

or

$$R_{\nu} = \frac{1}{3} E\left[\sum_{o}^{m}\sum_{o}^{m} A_{mn}\, 2mr^{2n+1}\left(\frac{L}{2}\right)^{2m-1}\right] \qquad (2.3.10)$$

Consider equation (2.3.4),

$$f(a)\sum_{o}^{m}(-1)^{m} + \sum_{o}^{m}\sum_{o}^{m} A_{mn}a^{2n+1}\left(\frac{L}{2}\right)^{2m} = 0$$

or

$$f(a) = \frac{\sum_{o}^{m}\sum_{o}^{m} A_{mn}a^{2n+1}\left(\frac{L}{2}\right)^{2m}}{\sum_{o}^{\infty}(-1)^{m+1}} \qquad (2.3.11)$$

The differential equations of equilibrium, from equations (2.2.11) and (2.2.12) of the previous section, become,

$$-\frac{1}{3} E\left[f''(r)\cos kz + \sum_{o}^{\infty}\sum_{o}^{\infty} A_{mn}2n(2n+1)r^{2n-1}z^{2m} + \frac{f'(r)}{r}\cos kz + \right.$$

$$+ \sum_{o}^{m}\sum_{o}^{m} A_{mn}(2n+1)r^{2n-1}z^{2m} - \frac{f(r)}{r^{2}}\cos kz - \sum_{o}^{\infty}\sum_{o}^{\infty} A_{mn}r^{2n}z^{2m}$$

$$\left. - f(r)k^{2}\cos kz + \sum_{o}^{m}\sum_{o}^{m} A_{mn}r^{2n+1}2m(2m-1)z^{2m-2}\right] = \left[1 + \frac{f(r)}{r}\cos kz\right.$$

$$\left. + \sum_{o}^{\infty}\sum_{o}^{\infty} A_{mn}r^{2n}z^{2m}\right]\left[1 + g(r)k\cos kz + \sum_{o}^{m}\sum_{o}^{m} B_{mn}(2m+1)r^{2n}z^{2m}\right]\frac{\partial p}{\partial r} -$$

$$- \left[g'(r)\sin kz + \sum_{0}^{\infty}\sum_{0}^{\infty} B_{mn}\, 2n r^{2n-1} z^{2m+1}\right]\left[1 + \frac{f(r)}{r}\cos kz + \sum_{0}^{\infty}\sum_{0}^{\infty} A_{mn} r^{2n} z^{2m}\right]\frac{\partial p}{\partial z} ,$$

(2.3.12)

and

$$- \frac{1}{3} E\left[g''(r)\sin kz + \sum_{0}^{m}\sum_{0}^{m} B_{mn}\, 2n(2n-1) r^{2n-2} z^{2m+1} + \frac{g'(r)}{r}\sin kz + \right.$$

$$\left. \sum_{0}^{m}\sum_{0}^{m} B_{mn}(2n) r^{2n-2} z^{2m+1} - g(r)k^2 \sin kz + \sum_{0}^{m}\sum_{0}^{m} B_{mn} r^{2n}(2m)(2m+1) z^{2m-1}\right] =$$

$$= -\left[1 + \frac{f(r)}{r}\cos kz + \sum_{0}^{m}\sum_{0}^{m} A_{mn} r^{2n} z^{2m}\right]\left[-f(r)k \sin kz + \right.$$

$$\left. + \sum_{0}^{m}\sum_{0}^{m} A_{mn} r^{2n+1} 2m z^{2m-1}\right]\frac{\partial p}{\partial r} +$$

$$+ \left[1 + f'(r)\cos kz + \sum_{0}^{m}\sum_{0}^{m} A_{mn}(2n+1) r^{2n} z^{2m}\right]\left[1 + \frac{f(r)}{r}\cos kz + \right.$$

$$\left. + \sum_{0}^{m}\sum_{0}^{m} A_{mn} r^{2n} z^{2m}\right]\frac{\partial p}{\partial z} . \qquad (2.3.13)$$

The incompressibility condition, equation (2.2.10) of the previous section, becomes

$$\left[1 + f'(r)\cos kz + \sum_{0}^{m}\sum_{0}^{m} A_{mn}(2n+1) r^{2n} z^{2m}\right]\left[1 + \frac{f(r)}{r}\cos kz + \sum_{0}^{m}\sum_{0}^{m} A_{mn} r^{2n} z^{2m}\right]\cdot$$

$$\left[1 + g(r)k \cos kz + \sum_{0}^{m}\sum_{0}^{m} B_{mn}(2m+1) r^{2n} z^{2m}\right] - \left[1 + \frac{f(r)}{r}\cos kz + \right.$$

$$\left. + \sum_{0}^{m}\sum_{0}^{m} A_{mn} r^{2n} z^{2m}\right]$$

$$\left[g'(r)\sin kz + \sum_{0}^{\infty}\sum_{0}^{\infty} B_{mn}\, 2n r^{2n-1} z^{2m+1}\right]\left[- f(r)\, k \sin kz + \right.$$

$$\left. + \sum_{0}^{\infty}\sum_{0}^{\infty} A_{mn}(2m) r^{2n+1} z^{2m-1}\right] \qquad \textbf{(2.3.14)}$$

Now, there are nine unknowns, $R_\nu(r,\frac{L}{2})$, $Z_\nu(r,\frac{L}{2})$, A_{mn}, $f(r)$, $g(r)$, $p(r,z)$, B_{mn}, $\frac{\partial p}{\partial r}$, and $\frac{\partial p}{\partial z}$ and there are nine algebraic equations which can be used to solve for these unknowns, equations 2.3.2, .4, .5, .6, .8, .10, .12, .13, and .14. Unfortunately, some of these equations, as can be easily seen, are non-linear algebraic equations and are also quite long. Therefore, due to the magnitude of work involved in the solution of these nine equations being much larger than the time available in which to devote to this solution, work on this aspect has ceased.

2.4 Theoretical Predictions of Strains

The strains on the surface ($r = a = 1$ in.) of the cylinder, for a given load, will be calculated from the deformations as predicted by Filon's theory. The deformations are given in equations (2.1.27) and (2.1.28) of section 2.1. The constants in these equations must be determined and can be found from equations (2.1.29) through (2.1.35). It has been found that Poisson's ratio for Solithane is 0.4 and in the following section on experimental results it has been determined from Table 4.1.1 that the modulus of elasticity of Solithane is 172.1 lb/in^2.

The constants have been found to be

$A = 245.8\ lb/in^2$

$\mu = 61.46\ lb/in^2$

$\gamma = .83331$

$\alpha_n = 1.571\ n$

$I_1(\alpha_1) = 1.035$

$I_0(\alpha_1) = 1.701$

$I_1(a_2) = 4.344$

$I_0(\alpha_2) = 5.314$

$I_1(\alpha_3) = 18.56$

$I_0(a_3) = 20.95$

$I_1(\alpha_4) = 81.46$

$I_0(a_4) = 88.84$

$\zeta = 17.12$, with calculations to n = 4

$f = -11.9556$

$g = -1.573$

$h = -10.442$

$u_0 = .000663Q$

$u_1 = .000816Q$

$u_2 = .000012Q$

$D = -.003696Q$

$E = -.0004212Q$

$F = .00103Q$

$w_0 = -.002757Q$

$W_1 = .00339Q$

$w_2 = -.000468Q$

$D^1 = -.00187Q$

$E^1 = .000468Q$

$F^1 = 0$

$C_1 = -.001069Q$

$C_2 = .0008498Q$

$C_3 = -.000139Q$

$C_4 = .00002617Q$

$A_{21} = .0036785Q$

$A_{22} = -.0010038Q$

$A_{23} = .00020785Q$

$A_{24} = -.00005995Q$

$A_{11} = .005314Q$

$A_{12} = -.001654Q$

$A_{13} = .0002788Q$

$A_{14} = -.000160l5Q$

Using the above constants, the deformation in the radial direction at the center of the surface of the cylinder, u(1,0), was found to be, with $Q = \frac{Q'}{\pi a^2} \equiv \frac{Q'}{\pi}$,

$$u(1,0) = 6.744 \times 10^{-4} \frac{Q'}{\pi}$$

Fromthe classical theory of elasticty $\varepsilon_{\theta\theta} = \frac{u}{r}$, therefore,

$$\varepsilon_{\theta\theta}(1,0) = \frac{u(1,0)}{1} = u(1,0).$$

Using the values for applied load, Q', that were used in the experiments, the following values for $\varepsilon_{\theta\theta}$ shown in Table 2.4.1 can be found.

Using the above constants, the derivative of the deformation in the axial direction with respect to z at r=1 and z=0 was found to be, $w'(1,0) = -9.802 \times 10^{-4} \frac{Q'}{\pi}$. From the classical theory of elasticity $\varepsilon_{zz} = \frac{\partial w}{\partial z}$. Using the proper values for Q' as above, ε_{zz}, shown in Table 2.4.2, can be found.

Q'(lbs)	$\varepsilon_{\theta\theta}(\times 10^{-4})$
0	0
6	12.88
12	25.76
18	38.64
24	51.52
30	64.40
36	77.28
42	90.16
48	103.04
54	115.92
60	128.80

Circumferential Strain for Various Values of Load
Table 2.4.1

Q'(lbs)	$-\varepsilon_{zz}(\times 10^{-4})$
0	0
6	30.48
12	60.96
18	91.44
24	121.92
30	152.40
36	182.88
42	213.36
48	243.84
54	274.32
60	304.80

Axial Strain for Various Values of Load
Table 2.4.2

CHAPTER 3

EXPERIMENTAL INVESTIGATION

3.1 Description of the Material

Solithane resin 113 is a urethane prepolymer which upon curing produces solid materials. Depending upon the selection and proportioning of the catalyst employed, cured materials can be formed which vary from soft, rubbery compounds, through a range of intermediate states, to products of a hard, extremely rigid nature.

DB castor oil was chosen as the catalyst in the preparation of specimens used in the experimental program here, DB castor oil is approximately 90% triglyceride of ricinoleic acid. This catalyst wgs mixed with the Solithane 113 in the manner described in the following section and the final product was a rubbery material of intermediate hardness.

Zak (10) has described the chemical aspects of Solithane resin 113 in detail.

3.2 Specimen Preparation

The repeatability of test results from one test specimen to another depends, to a large extent, on the modus operandi employed in the preparation of the specimens. Great care was taken, therefore, in the preparation of test specimens. The specimens utilized in this testing program were produced by the following method.

The molds were of cylindrical shape, as shown in Figure 2. All parts of each mold were made of aluminum. The plate on the bottom of each mold was machined out so that the cylindrical portion of the mold

would fit into it. The upper plate was machined with a piston-like projection that would fit into the top of the cylindrical portion of the mold. The upper and lower end plates were attached together with three springs. These springs caused a force which pulled the upper piston-like plate down against the upper surface of the liquid. This was done in order to compensate for the contraction of the liquid material during curing. Without an end plate on the upper surface, shrinkage of the material during curing would have caused the surface of the cured material to be somewhat concave. Also, the texture of the upper surface compared with the texture of the lower surface will differ unless a plate is used on both ends. For studies where friction is involved, the surface textures must be the same.

Four molds were used for each batch of specimens prepared. The molds were cleaned thoroughly with a solvent. They were then sprayed with two mold releases, Slipicone, a product of Dow Chemical Company, and Fluoroglide, a Chemplast Company product. Preheating each mold was accomplished by placing them in an oven set at 185°F. for about three hours. The molds were preheated so that their temperature would equal that of the mixture which was going to be poured into them.

While the molds were preheating, the basic materials used in the specimen preparation were mixed in the following manner. Of the total weight of mixture needed for one particular batch, four parts by weight of castor oil were vacuumed for two hours in order to remove as much air as possible from the liquid. The air was removed in order that no bubbles would form in the final solid specimens. Three parts, by weight, of Solithane 113 were added to the castor oil and the

mixture of Solithane and castor oil was heated on a hot plate at a temperature of 130°F and simultaneously vacuumed for a period of ten minutes. At the end of the ten minute time lapse, a magnetically operated stirring device was activated and the heating, vacuuming, and stirring were continued for another ten minutes. At the end of the second ten minutes, the heat was reduced to 120°F and the vacuuming and stirring were continued for a third ten minute period. The object of the heating and vacuuming was to remove the air bubbles and the object of the stirring was to thoroughly mix the Solithane and castor oil.

The preheated molds, without their tops, were removed from the oven and the mixture was poured into them to a predetermined level. The filled molds were then placed in a vacuum chamber and the chamber was evacuated for twenty minutes in order to remove air that might have entered the mixture during the pouring process. The tops were placed on the molds properly and the molds were placed into an oven of special design, set at 250°F.

The design of this oven, which is shown in Figure 3, was such that the molds could be rotated continually during the curing time. This was done by attaching an electric motor, whose original 1725 rpms were reduced appropriately to about ten rpms, to the protrusion of a one-inch aluminum rod fromthe inside of the oven. The molds were affixed to this rotating rod and were therefore rotated also. This simultaneous rotation and heating was continued for two hours.

The molds were removed from the oven and their tops and bottoms removed. The specimens were pressed out of the cylindrical portions

of their molds. The mold release that had adhered to the specimens was removed by rubbing with a soft cloth saturated with solvent. The specimens were then labeled appropriately as to batch and aged for at least three days before being used in experiments.

One precautionary measure was taken throughout the entire preparation of specimens and also during storage of the final products. Since Solithane 113 and castor oil are very hygroscopic, the time that the liquids were exposed to the atmosphere, during specimen preparation, was reduced to a minimum. For instance, in draining the liquids from their storage containers, nitrogen gas was used as a forcing pressure in the drums. Also, the final specimens were stored at all times before experimentation in dessicators where the dessicant used was calcium sulfate ($CaSO_4$). In addition, the experimental testing laboratory had a controlled atmosphere, i.e., constant temperature at 74°F and constant relative humidity at 45%. Therefore, any change that might take place in the material due to temperature or humidity while the experiments were being conducted was equal in magnitude.

3.3 Experimental Apparatus and Procedure

Because Solithane 113 is a very soft, rubber-like material, a method of strain measurement in which there is no physical contact between the specimen and the measuring device must be utilized. Should a device, i.e., bonded electrical strain gages, be used where such physical contact occurs, the material properties of the specimen in the region of contact, and therefore, in the region of strain measurement may be altered.

"he strain, as yielded by the imposed testing conditions, may be non-uniform, although it is assumed to be uniform for simplicity of theoretical derivations of the strains on the surface. This non-uniformity is due to the bulging of the curved portion of the specimen when the axial load is applied. Local strain measurements are therefore needed so that a suitable strain analysis can be performed.

A method of measuring strains that will eliminate the two above mentioned experimental difficulties is the moiré fringe method. The moire method measures strains by using the principle of mechanical interference of light. Two superposed grids of alternate light and dark lines will cause interference patterns or fringes when there is a relative rotation of the grids, a difference in pitch of the grids, a displacement between the grids or any combination of relative rotation, pitch difference, or displacement. The name, moiré, is the French word meaning watered-silk which describes the appearance of the fringes. The proper analysis, at a desired point, of the fringe pattern will yield the strain at that point. No physical contact is necessary when using the moiré method.

The grids used in the testing were obtained by photographic and diazo printing techniques. A Ronchi ruling on a one inch by two inch by one-quarter of an inch, piece of'glass was used as the original grid. Ronchi rulings are unique in that the width of the dark lines are equal to the width of the light lines. The Ronchi ruling was used to contact print alternate light and dark lines onto Kodak, Contrast Process Ortho film sheets, a high contrast, fine grain orthochromatic, antihalation film. The original grid had a pitch of 500

lines per inch and consequently all of the grids produced from it were of the same pitch.

As noted, there are two grids employed in the moire method. One grid, the model grid, is affixed to the surface of the specimen to be tested in the desired area of strain measurement. The second grid is superposed on the model grid during testing and is called the master grid.

The master grid, in this case, is simply a photographic negative of the Ronchi ruling. A photographic negative was used as a master grid because its flexibility was essential when the grid was superposed on the curved surface of the cylindrical specimens.

For most materials and specimen shapes, the model grid can be printed directly onto the specimen surface at the desired location of strain analysis. Unfortunately, Solithane 113 reacts chemically with the solutions usually employed in printing processes. Therefore, a diazo printing technique had to be used, A formula for making diazo solution and a description of the diazo printing process can be found in Appendix B.

Since the diazo technique involves contact printing and to contact print directly onto the surface of a cylindrical specimen would be difficult, a bonded type gage was developed. Solithane was molded, by the method described previously, into a sheet 0.03 inches thick. The sheet was cut into smaller two inch by two inch squares. In order to provide contrast with the dark lines resulting fromthe diazo process, a ten to one mixture of white latex paint and liquid latex rubber was sprayed onto the surface of the small thin sheet with an

artist's air brush. The liquid latex rubber was added to the latex paint to give the paint sufficient elasticity in order to prevent cracking during elongation of the model grid. Immediately after the paint and latex mixture was applied, the diazo solution was sprayed onto the sheet with the air brush. The diazo and paint-latex mixture was then allowed to dry, usually two to three days. Drying was done in a dessicator where no light could penetrate in order that the ultra-violet light present in the sunlight could not react with the diazo solution on the thin sheet.

When dried, the coated thin sheet was placed in a vacuum printing frame with a photographic negative of the Ronchi ruling superposed on the thin sheet. A vacuum printing frame was used to ensure intimate contact between the thin sheet and the superposed negative during exposure. With the printing frame in operation, the diazo coating on the thin sheet was exposed, throught the negative, to the ultra-violet light source. The development process then took place as described in Appendix B.

After development, the thin sheet was cut to the proper size and was glued to the surface of the cylindrical specimen in the area of desired strain measurement and with proper orientation with respect to the grid lines. The glue used was General Electric #108 silicone cement., It is a low modulus cement as was needed because a cement with a modulus higher than that of the specimen would influence the deformation of the grid adversely. The silicone rubber cement was cured for at least one day before the specimen was tested.

Both tension and compression specimens were tested in a Tinius Olsen universal testing machine. This machine is shown in Figure 4. The maximum load available is twelve thousand pounds. Altogether, twelve load ranges are available for use. Tension experiments were conducted using the twelve pound range and compression experiments were run using the 120 pound range. The maximum crosshead speed is twenty inches per minute and is continuously variable. Both compression and tension experiments were carried out using a crosshead speed of one-quarter of one inch per minute. The load being applied to the specimen is registered on a moving strip chart that is calibrated from zero to one hundred percent of the load range being utilized.

The tension specimen used was of the flat type, as shown in Figure 5. Its dimensions, also noted in Figure 5, conform to the JANAF standards. On the tension specimens the thin sheet with printed grid lines was glued to the test section. The thin sheet was glued with the grid lines perpendicular to the direction of the applied load. The tension specimen was held in the testing machine by two grips like the one shown in Figure 6. The compression specimen used was cylindrical in shape. As shown in Figure 7, its length is twice its diameter. These dimensions were chosen because a specimen of this size exhibits bulging when compressed but is not difficult to handle experimentally.

The thin sheet was oriented on the cylindrical surface in two ways. For measuring axial strain the grid lines were oriented with the direction of the lines perpendicular to the direction of the

applied load. For measuring circumferential strain the grid lines were oriented with the direction of the lines parallel to the direction of the applied load.

A cage-like apparatus, shown in Figure 4, was constructed so that compression could be applied to the specimen by operating the testing machine as though a tension experiment were being conducted.

The following parts of the discussion on experimental procedure apply to tension and compression experiments alike.

The thin sheeted area of the specimen was coated with a thin layer of petroleum jelly. The purpose of the jelly was to hold the master grid in place during the experiment. In the case of the cylindrical specimens, the master grid was held to the cylindrical surface by a girdle-like arrangement of three elastic bands. The master grid being affixed to the specimen, the air bubbles that had formed in the jelly between the grid and the thin sheet were removed by pressing the master grid with a soft cloth.

The tension or compression specimen was placed in the appropriate grips or apparatus and the proper testing machine variables, as specified above, were set. A Nikon F camera on a tripod, loaded with Kodak Tri X Pan thirty five millimeter film and equipped with extension tubes for close up photography, was positioned properly. The camera was used to photograph the moiré fringes that had formed during experiments so that an analysis of the fringes could be performed. For proper illumination of the fringes during experiments, two photographic flood lamps were used.

With the testing machine in operation, pictures of the fringes formed during deformations at specific applied loads were taken. The film of the fringe patterns was developed. The film negatives were then enlarged onto Kodak F5 or F4 Kodabromide photographic paper. Each enlargement was labeled properly according to test number and the load corresponding to the fringe pattern.

The method of analysis of each fringe pattern is discussed in the following section.

3.4 Moiré Fringe Theory

The moire fringe method of strain analysis is relatively new. Although the theory of diffraction gratings and of their manufacture date back to Lord Rayleigh (5), 1874, the application of diffraction gratings to strain measurement began with M. Dantu (2) in 1940. Since then, the theory involved in the analysis of the fringes formed in the moiré method as well as the experimental techniques involved have advanced rapidly.

The formation of moire fringes is a mechanical phenomenon that consists of alternating light and dark regions. The fringes formed are not an optical phenomenon in the sense that no basic laws of optics are involved in their formation. Fringes result when one array of dots or solid lines is superposed on a second somewhat similar array of dots or solid lines, hereafter referred to as grids. The fringes are caused by a difference in the pitch of the two grids, a relative rotation of the grids, paralax caused by a displacement between the grids, or any combination of a difference in pitch, a relative rotation, or paralax. Since fringes can result from relative

differences in pitch and rotation, this phenomenon can be employed to measure strain,

Two grids are used in the moiré method of strain analysis, a master grid and a model grid. The master grid is a fixed array of straight, parallel, alternate light and dark lines with pitch, p, defined as the distance between adjacent light or dark lines of the grid. The model grid, a similar array of lines, is affixed to the specimen being tested so that as the specimen deforms under a load, the grid will deform with it and, therefore, will have a distorted pitch, p'. With the master grid superposed on the model grid, fringes will be formed as the model grid distorts along with the specimen. Although the analysis is not necessarily limited to straight, parallel lines, this analysis will be because straight, parallel lined grids were used in the experimental part of this work.

Figure 8 shows a close up of the formation of moiré fringes by a relative rotation and a difference in pitch of two grids that are composed of straight, parallel lines. The r,s coordinate system is taken to be coincident with the master grid as shown.

The acute angle between the master and model grid lines is denoted by θ. The angle ϕ is between the master grid lines and the fringe and is measured in the same direction as θ and may be acute or obtuse. The distance between the centers of the adjacent fringes is 6. The pitch of the master grid is p and the pitch of the model grid is p'.

Then, from geometrical considerations and by assuming either a homogeneous deformation or a sufficiently small element of a

nonhomogeneous deformation field, the equations for strain can be derived (4). True strain in the r-axis direction is

$$[\varepsilon_r]_t = \beta_\delta \left(\frac{p}{\delta}\right), \tag{3.4.1}$$

and conventional or nominal strain in the r-axis direction is

$$[\varepsilon_r]_c = \frac{\beta_\delta \left(\frac{p}{\delta}\right)}{1 - \frac{\beta_\delta p}{\delta}} \tag{3.4.2}$$

where

$$\beta_\delta = \frac{\delta}{p}\left[1 - \sqrt{\left(\frac{p}{\delta}\right)^2 + 2\left(\frac{p}{\delta}\right)\cos\phi + 1}\right] \tag{3.4.3}$$

It should be noted that the strain determined is in the direction perpendicular to the direction of the grid lines of the master grid.

As can be seen from equations (3.4.1), (3.4.2), and (3.4.3), we need to know δ, p, and the magnitude and direction of ϕ in order to determine the strain and to find if the strain is compressive or tensile. In the problem in this discussion, $\phi \cong 180°$ and, therefore, equation (3.4.3) becomes

$$\beta_\delta = \frac{\delta}{p}\left[1 - \sqrt{\left(\frac{p}{\delta}\right)^2 + 2\left(\frac{p}{\delta}\right) + 1}\right]$$

$$\beta_\delta = \frac{\delta}{p}\left[1 - \sqrt{\left(\frac{p}{\delta} + 1\right)^2}\right]$$

$$\beta_\delta = \frac{\delta}{p}\left[1 - \frac{p}{\delta} - 1\right]$$

$$\underline{\beta_\delta = -1}\ .$$

Therefore, equations (3.4.1) and (3.4.2) become

$$[\varepsilon_r]_t = \frac{p}{\delta} \tag{3.4.4}$$

and

$$[\varepsilon_r] = \frac{p}{\underline{p}} \tag{3.4.5}$$

In equations (3.4.4) and (3.4.5), p, the pitch of the master grid is known and, therefore, all that must be determined in order to find the strain is the distance between the centers of the fringes. In order to find 6 from photographs of moiré fringes, a graphical approach is taken. A line is drawn, in the proper direction, across a series of fringes which includes the point at which strain is to be measured. A plot of the accumulated fringe distances, from any convenient point, versus the fringe number is made. Fringes are numbered consecutively with zero fringe as the point at which the accumulated fringe distance measurements are originated. A smooth curve is drawn through the plotted points. The slope of this curve at any point gives the value of 6, in inches per fringe, at that point, With the known value of δ at any point, the value of the strain at that point can be found by using equations (3.4.4) and (3.4.5).

Equations for true strain in terms of ϕ and the distance between adjacent fringe centers, measured along the coordinate axes, r and s, can also be derived (4), and are

$$[\varepsilon_r]_t = \beta_r\left[\frac{p}{\delta_r}\right] = \beta_s\left[\frac{p}{\delta_s}\right] \tag{3.4.6}$$

where

$$\beta_r = \frac{\delta_r}{p}\left[1 - \sqrt{\left(\frac{p}{\delta_r}\right)^2 \frac{1}{\cot^2\phi} + 2c\left(\frac{p}{\delta_r}\right) + 1}\right]$$

for

$$c = \begin{matrix} 1, 0 < \phi < \frac{\pi}{2} \\ -1, \frac{\pi}{2} < \phi < \pi \end{matrix} \qquad (3.4.7)$$

and

$$\beta_s = \frac{\delta_s}{p}\left[1 - \frac{1}{\sin\phi}\sqrt{\left(\frac{p}{\delta_s}\right)^2 + \frac{p}{\delta_s}\sin 2\phi + \sin^2\phi}\right] \qquad (3.4.8)$$

It is sometimes more accurate to measure accumulated fringe distances in one of the coordinate axis directions rather than to measure directly. When this is true, equations (3.4.6), (3.4.7), and (3.4.8) are used to calculate strain.

If rotation at a point is to be determined, the equations

$$\sin\theta = \alpha_s\left(\frac{p}{\delta_s}\right)$$

and

$$\text{sine} = a_r\left(\frac{p}{\delta_r}\right)$$

where

$$\alpha_s = \sqrt{\frac{\frac{\delta_s}{p}}{1 + \left(\frac{\delta_s}{p} + \cot+\right]2}}$$

and

$$a_r = \frac{\frac{\delta_r}{P}}{\sqrt{1 + \left[1 + c\frac{\delta_r}{p}\right]^2 \cot^2\phi}}$$

if

$$c = \begin{cases} 1, & 0 < \phi < \frac{\pi}{2} \\ -1, & \frac{\pi}{2} < \phi < \pi \end{cases}$$

can be used.

Moiré patterns may also be interpreted as a function of displacements as shown by Sciammarella and Durelli (7) and in an earlier work by J.D.C. Crisp (1). This interpretation of moiré fringes is based on the fact that the fringes are the loci of points presenting the same relative displacement in the direction normal to the master grid lines.

In this method, a Cartesian system of axes, x and y, is used as a reference system, as shown in Figure 9. The component of displacement in the x-axis direction is u and the component of displacement in the y-axis direction is v.

A function of two variables, $\phi_i(x,y)$, is the component of displacement of a point in a two-dimensional continuous medium parallel to a reference direction. The subscript, i, is 1 if the reference direction is the x-axis and subscript, i, is 2 if the reference direction is the y-axis. The function $z = \phi_i(x,y)$, in Cartesian coordinates, represents a surface.

To determine strains from displacements, it is necessary to compute the derivatives of the displacements. To compute the partial derivatives of $\phi_i(x,y)$, the curves of intersection of the surface with planes of equations $x = c_1$ and $y = c_2$ can be drawn, where c_1 and c_2 are constants. The procedure used to obtain a partial derivative is illustrated in Figure 9. The horizontal position of each point of

intersection of the moire' fringes with the line AB (trace of the intersecting plane) is first projected on the base line CD. The orders of fringes are read from the moire' fringes and distances equal to np are scaled up from the base line. A line drawn through the points, thus plotted, defines the cross-section. The slope of this curve, at a point, gives the derivative

$$\frac{\partial \phi_i}{\partial y} \quad .$$

If the preceding data are plotted directly from the moiré pattern, the results obtained correspond to the Eulerian description of strain. For the Lagrangian description, there are two possible solutions. Assume that the patterns corresponding to two orthogonal directions have been determined. A point, p_o, of initial coordinates x_o and y_o moves, after deformation, to point p, with coordinates x and y. If the components of the displacements experienced by the point p_o are u and v,

$$xo = x_1 - u$$

and

$$y_o = y_1 - v \quad .$$

By using these equations, it is possible to obtain the necessary data to replot the moire fringes referred to the initial configuration.

Another possibility is that the derivative of u with respect to x_o can be expressed as a function of the derivative of u with respect to x, as follows,

$$\frac{\partial u}{\partial x_o} = \frac{\partial u/\partial x_1}{1 - \partial u/\partial x_1} \quad .$$

All of the partial derivatives of the displacements with respect to the initial coordinates can be put into the above form. Since the partial derivatives of the displacements with respect to the final coordinates can be found, $\partial u/\partial x_o$, etc. can be found and the Lagrangian strains can therefore be found.

A third method for analyzing strains from moiré fringes has been developed recently by Sciammarella (8). This method of analysis utilizes the light intensity variations of the moiré fringes. The new theory generalizes the optical law that relates the displacement field to the moire' fringe pattern. This yields a continuous relationship between displacements and light intensity. Until this theory was developed, a discontinuous relationship existed. Because of the continuous aspect of the light intensity variation method, the precision of moire' fringe analysis has been increased.

The relationship between the displacement at a point and its light intensity has been shown by Sciammarella to be

$$u = \left(\frac{1}{2\pi} \arccos \frac{I - I_o}{\mp I_1}\right) P \qquad (3.4.9)$$

where

p is the master grid bitch,

I is the light intensity at a point,

I_o is the image average background light intensity, and

I_1 is the light intensity amplitude of the image first harmonic,

The equipment used to measure the light intensity variations consists of a photocell mounted behind a small circular hole in the focal plane of a projecting system. The photocell must also be mounted on a

traveling carriage. A film of the fringes to be analyzed is then inserted between the photocell and a lens system. The photocell is then moved over the section of the fringes that are of interest and the resulting output is recorded on an x-y plotter. A sample output is shown in Figure 10.

In order to compute the displacement corresponding to a point, P, as shown in Figure 10, it is necessary first to determine the integral number of fringes prior to point P. The fractional displacement is then determined by using equation (3.4.9) with $I_o = I_1 = \frac{AB}{2}$ and $I = cp$. The fractional displacement is then,

$$\Delta u = \left[\frac{1}{2\pi} \text{ arc cos } \left(\frac{2CP}{AB} - 1\right)\right] p.$$

The theoretical minimum displacement sensitivity for the light intensity variation method as calculated by Sciammarella (8) is

$$Au = 0.0012 \text{ p.}$$

The minimum strain measurable when using the geometrical approach or the displacement function method is a function of the gage length employed and the number of lines per inch on the master grid. From Figure 5 of the paper by Crisp (1), the minimum measurable strain can be seen to be approximately 0.002 inches per inch for a gage length of one inch and a master grid with 500 lines per inch as was used in the experiments in this work.

The errors involved in the three moire strain analysis methods have been set down by Sciammarella. For the geometrical and displacement function methods, a bound in the error involved in strain

measurement when using a times 10 magnifying glass to read distances will be

$$\left|\frac{d\varepsilon}{\varepsilon}\right| \quad 4\% \ .$$

The error due to the measuring apparatus used in the light intensity variation method will be

$$\left|\frac{d\varepsilon}{\varepsilon}\right| = 22\% \ .$$

These errors are for measurements only and do not include errors in grid spacing, et cetera.

It is apparent that the light intensity variation method is far superior in both sensitivity and minimum error in measurements. In addition, as was previously mentioned, the light intensity variation method yields a continuous quantity to be measured where the two other methods yield discontinuous measurable quantities. However, the expensive equipment used and the time involved in perfecting the method precluded the use of the light intensity variation method in this work. The geometrical method of moiré fringe analysis was chosen for use here and the light intensity variation method and the displacement function method were included in this discussion for informative and comparative reasons.

A sample calculation of the strain from a moiré pattern can be found in Appendix C.

CHAPTER 4

EXPERIMENTAL RESULTS AND DISCUSSION

4.1 Tension Experiments

Tension experiments were conducted with several objectives in mind: (i.) to gain experience with the moire fringe method of strain measurement, (ii.) to verify experimental results obtained with the moire method with results obtained when using another method of analysis, and (iii.) to obtain a modulus of elasticity that could be used in the theoretical analysis.

The third objective was reached by measuring the strain in the direction of the load application at various intervals of load. Graphs of the true stress, $\sigma_t = \left(\frac{P}{A}\right)\lambda$, versus extension ratio, λ, were plotted and the slope of the curve was taken as the modulus of elasticity, as shown in Appendix C. The moduli obtained by testing eight different specimens are shown in Table 4.1.1 below. As can be seen there is a large variation in moduli from one specimen to another, therefore, an average value was found. This value of these eight moduli was found to be 172.1 lb/in^2 and this is the value that was used in the theoretical predictions of strains found in Chapter Two, Section Four.

The second objective was met by comparing the moduli obtained above with the moduli that was found by clip-gage measurements. The modulus obtained in the second fashion is 175.0 lb/in^2 as shown in an unpublished work completed here. The percent difference between the two is found to be 1.65%.

Specimen No.	Modulus (lb/in^2)
165 E	190.5
166 E	210.0
167 E	143.0
231 ψ	162.5
232 ψ	141.2
233 ψ	211.0
236 ψ	153.3
237 ψ	165.0

Experimentally Determined Values of Moduli
for Different Specimens

Table 4.1.1.

4.2 Compression Experiments

Uniaxial compression tests were performed on right, circular cylinders of moderate length which were made of cured Solithane 113. The axial and circumferential strains that existed on the surfaces of the cylinder at the axial center were measured by means of the moiré method. The range of strains measured was determined by the characteristics of the moird grids used. The range of strains measured was approximately .001 in/in to .06 in/in.

Two types of boundary conditions were imposed on the ends of the cylinders. The first type imposed was such that the radial deformations of: the end surfaces was zero. The second type imposed was such that the radial deformation of the end surfaces was not zero, i.e., lubricant was applied to the ends in order that the friction between the compression plates and the ends of the cylinders was nearly zero.

4.3 Conclusions

1. For relatively small compressive loads, the axial and circumferential strains are equal in magnitude for lubricated and non-lubricated ends, as shown in Figures 11, 12, 13, and 14.

2. With lubricated ends, the axial strain is smaller than for non-lubricated ends when relatively large compressive loads are applied to the specimens. Also, as the magnitude of the compressive load is increased, the difference in strains increases, as shown in Figures 13 and 14.

3. For a given, relatively large compressive load, the circumferential strain on a cylinder with lubricated ends is less than on a cylinder with non-lubricated ends, as shown in Figures 11 and 12.

4. Strains in the axial direction are larger than strains in the circumferential direction, as shown in Figures 11, 12, 13, and 14.

5. A smooth curve fromtension to compression seems to exist although further study is needed to verify this, as shown in Figure 15.

6. The experimental results did not agree at all with the theoretical results as derived by Filon (3), as shown in Figures 11 and 13. This was, however, expected because in the theoretical derivations the assumption of small strains was made and in the experimental work the strains were relatively large.

7. The Poisson ratio was found to be 0.4773 for a strain rate of .25 in/min and at a load of 30 lbs. This agrees well with the assumption of incompressibility, where Poisson ratio is taken to be 0.5, used in the derivation of the equations describing large elastic deformations.

4.4 Suggestions for Further Research

On the basis of the research conducted and the results obtained the author makes the following suggestions for further research:

1. That a study be made of the small strains that exist when small loads are applied to the specimen.

2. That a study be made of the large strains that exist when large loads are applied to the specimen.

3. That a study be made of the strains that exist at various points on the surface of the cylinder.

4. That a solution to the equations describing the strain at any point in the cylinder for a given load be found.

REFERENCES

1. Crisp, J.D.C., "The Measurement of Plane Strains by a Photo-screen Method," Proc. SESA, Vol. 15, No. 1, 1957.

2. Dantu, M., "Determination Experimentale des Flexions dans une Plaque Plane," Memoirs et Documents des Ingenieurs des Ponts et Chanssees, 1940.

3. Filon, L.N.G., "On the Elastic Equilibrium of Circular Cylinders under Certain Practical Systems of Loads," Phil. Trans. Roy. Soc., Ser. A, v. 198, 1902.

4. Morse, S., Durelli, A., Sciammarella, C., "Geometry of Moiré Fringes in Strain Analysis," Proc. ASCE, August, 1960.

5. Rayleigh, Lord, "On the Manufacture and Theory of Diffraction Gratings," Scientific Papers of Lord Rayleigh, Cambridge Univ. Press, Vol. 1, p. 209, 1874.

6. Rivlin, R.S., "Large Elastic Deformations of Isotropic Materials," Phil. Trans. Roy. Soc., Ser. A, v. 240, 1948.

7. Sciammarella, C., and Durelli, A., "Moiré Fringes as a Means of Analyzing Strains," Proc. ASCE, EM 1, Feb., 1961.

8. Sciammarella, C., "Basic Optic Law in the Interpretation of Moire Patterns Applied to the Analysis of Strains," Part 1 and 2, Experimental Mechanics, May and June, 1965.

9. Timoshenko, S. and Goodier, J., Theory of Elasticity, McGraw-Hill Book Co., Inc., 2nd ed., 1951.

10. Zak, A.R., "Multiaxial Failure of Viscoelastic Materials," Aerospace Research Laboratories, ARL64-144, Sept., 1964.

APPENDIX A

MATHEMATICAL CALCULATIONS

The equation to be solved is

$$\left[\frac{d^2R_2}{dr^2} + \frac{1}{r}\frac{dR_2}{dr} - \left(\frac{1}{r^2} + k^2\right)R_2\right]^2 = 0$$

Let

$$R_2 = r^{\mu}\{a_0 + a_1 r + a_2 r^2 + \ldots\}.$$

Then

$$\frac{1}{r}\frac{dR_2}{dr} = r^{\mu}\{a_0\mu r^{-2} + a_1(\mu+1)r^{-1} + a_2(\mu+2) + a_3(\mu+3)r + a_4(\mu+4)r^2 + \ldots\}$$

$$\frac{d^2R_2}{dr^2} = r^{\mu}\{a_0(\mu-1)\mu r^{-2} + a_1\mu(\mu+1)r^{-1} + a_2(\mu+1)(\mu+2) + a_3(\mu+2)(\mu+3)r + a_4(\mu+3)(\mu+4)r^2 + \ldots\}.$$

First let us solve the following equation.

$$\frac{d^2R}{dr^2} + \frac{1}{r}\frac{dR}{dr} - \left(\frac{1}{r^2} + k^2\right)R = 0 \qquad (1)$$

Let

$$R = r^{\mu}\{a_0 + a_1 r + a_2 r^2 + a_3 r^3 + a_4 r^4 + \ldots\}. \qquad (2)$$

Then

$$\frac{1}{r}\frac{dR}{dr} = r^{\mu}\{\mu\, a_0 r^{-2} + a_1(\mu+1)r^{-1} + a_2(\mu+2) + a_3(\mu+3)r + a_4(\mu+4)r^2 + \ldots\}. \qquad (3)$$

$$\frac{d^2R}{dr^2} = r^{\mu}\{a_0(\mu-1)\mu r^{-2} + a_1\mu(\mu+1)r^{-1} + a_2(\mu+1)(\mu+2) + a_3(\mu+2)(\mu+3)r + a_4(\mu+3)(\mu+4)r^2 + \ldots\}, \tag{4}$$

Substitute (2), (3), and (4) into eqn. (1)

$$r^{\mu}\{a_0(\mu-1)\mu r^{-2} + a_1\mu(\mu+1)r^{-1} + a_2(\mu+1)(\mu+2) + a_3(\mu+2)(\mu+3)r + a_4(\mu+3)(\mu+4)r^2 + \ldots + \mu\, a_0r^{-2} + a_1(\mu+1)r^{-1} + a_2(\mu+2) + a_3(\mu+3)r + a_4(\mu+4)r^2 + \ldots - a_0r^{-2} - a_1r^{-1} - a_2 - a_3r - a_4r^2 - \ldots - a_0k^2 - a_1rk^2 - a_2r^2k^2 - a_3r^3k^2 - a_4r^4k^2 - \ldots\} = 0$$

Equate coefficients of equal powered r's.

$r^{-2} \rightarrow$

$$a_0(\mu-1)\mu + a_0\mu - a_0 = 0$$

$$a_0\mu^2 - a_0\mu + a_0\mu - a_0 = 0 \tag{5}$$

$$\underline{a_0(\mu^2 - 1) = 0}$$

$r^{-1} \rightarrow$

$$a_1\mu(\mu+1) + a_1(\mu+1) - a_1 = 0$$

$$a_1\mu^2 + a_1\mu + a_1\mu + a_1 - a_1 = 0 \tag{6}$$

$$\underline{a_1\mu(\mu+2) = 0}$$

$r^0 \rightarrow$

$$a_2(\mu+1)(\mu+2) + a_2(\mu+2) - a_2 - a_0k^2 = 0$$

$$a_2\mu^2 + a_2 3\mu + a_2 2 + a_2\mu + a_2 2 - a_2 - a_0k^2 = 0$$

$$\underline{a_2(\mu+3)(\mu+1) - a_0k^2 = 0} \tag{7}$$

$$r \rightarrow \quad a_3(\mu+2)(\mu+3) + a_3(\mu+3) - a_3 - a_1k^2 = 0$$

$$a_3\mu^2 + a_35\mu + a_36 + a_3\mu + a_33 - a_3 - a_1k^2 = 0$$

$$\underline{a_3(\mu+4)(\mu+2) - a_1k^2 = 0} \qquad (8)$$

$$r^2 \rightarrow \quad a_4(\mu+3)(\mu+4) + a_4(\mu+4) - a_4 - a_2k^2 = 0$$

$$a_4\mu^2 + a_47\mu + a_412 + a_4\mu + a_44 - a_4 - a_2k^2 = 0$$

$$\underline{a_4(\mu+3)(\mu+5) - a_2k^2 = 0} \qquad (9)$$

Or, looking at (5), (6), (7), (8), and (9) tpgether

$$a_0(\mu^2-1) = 0$$

$$a_1\mu(\mu+2) = 0$$

$$a_2(\mu+3)(\mu+1) - a_0k^2 = 0$$

$$a_3(\mu+4)(\mu+2) - a_1k^2 = 0$$

$$a_4(\mu+3)(\mu+5) - a_2k^2 = 0 \ .$$

If $a_0 \neq 0$, $\mu = \pm 1$ from equation (5); $a_1 = 0$; $a_3 = a_5 = a_7 = \ldots = 0$, and from equation (7)

$$a_2 = a_0 \frac{k^2}{(\mu+3)(\mu+1)}$$

and equation (9)

$$a_4 = a_0 \frac{k^4}{(\mu+3)^2(\mu+1)(\mu+5)}$$

Substituting these values of a_2, a_4 etc. into equation (2)

$$R = r^\mu\left\{a_0 + a_0\frac{k^2r^2}{(\mu+3)(\mu+1)} + a_0\frac{k^4r^4}{(\mu+1)(\mu+3)^2(\mu+5)} + \ldots\right\}$$

Now, let $\mu = 1$, $a_0 = k/2$

$$R = \frac{1}{2} kr + \frac{1}{16} k^3 r^3 + \frac{1}{384} k^5 r^5 + \ldots$$

$$\boxed{R_1 = I_1(kr)}$$

The solution is invalid for $\mu = -1$ because R then blows up.

Instead of showing how to solve for the second solution of the differential equation, $R_2 = K_1(kr)$, let us prove, by using the Wronskian determihant, that $K_1(kr)$ is a linearly independent solution of the differential equation.

It is known that, if y_1 and y_2 are two solutions of a linear differential equation of the second order, and if y_1' and y_2' denote their derivations with respect to the independent variable, then the solutions are linearly independent if the Wronskian determinant

$$\begin{vmatrix} y_1 & y_2 \\ y_1' & y_2' \end{vmatrix}$$

does not vanish identically.

We have that

$$y_1 = R_1 = I_1(kr)$$
$$y_2 = R_2 = K_1(kr)$$
$$y_1' = k\, I_1'(kr)$$
$$y_2' = k\, K_1'(kr).$$

Therefore,

$$\begin{vmatrix} I_1(kr) & K_1(kr) \\ k\,I_1'(kr) & k\,K_1'(kr) \end{vmatrix} =$$

$$k\,I_1(kr)\,K_1'(kr) - k\,I_1'(kr)\,K_1(kr) =$$

$$k\,(I_1(kr)\,K_1'(kr) - I_1'(kr)\,K_1(kr)\,.$$

But it is known that

$$I_1(kr)\,K_1'(kr) - I_1'(kr)\,K_1(kr) = -\frac{1}{kr}$$

so that

$$k\left(-\frac{1}{kr}\right) = -\frac{1}{r}\,.$$

Then $I_1(kr)$ and $K_1(kr)$ are linearly independent solutions of the original differential equations.

Returning to the original equation to be solved,

$$\left[\frac{d^2}{dr^2} + \frac{1}{r}\frac{d}{dr} - \left(\frac{1}{r^2} + k^2\right)\right]^2 R_2 = 0. \tag{10}$$

$$\left[\frac{d^2}{dr^2} + \frac{1}{r}\frac{d}{dr} - \left(\frac{1}{r^2} + k^2\right)\right]\left[\frac{d^2}{dr^2} + \frac{1}{r}\frac{d}{dr} - \left(\frac{1}{r^2} + k^2\right)\right] R_2 = 0$$

Let

$$\left[\frac{d^2}{dr^2} + \frac{1}{r}\frac{d}{dr} - \left(\frac{1}{r^2} + k^2\right)\right] R_2 = \phi(r).$$

Then

$$\left[\frac{d^2}{dr^2} + \frac{1}{r}\frac{d}{dr} - \left(\frac{1}{r^2} + k^2\right)\right] \phi(r) = 0$$

where

$$\phi(r) = A\, I_1(kr) + B\, K_1(kr)$$

or

$$\phi(r) = A\, I_1(kr); \quad \phi(r) = B\, K_1(kr).$$

Then

$$\left[\frac{d^2R_2}{dr^2} + \frac{1}{r}\frac{dR_2}{dr} - \left(\frac{1}{r^2} + k^2\right)R_2\right] = A\, I_1(kr). \tag{11}$$

Let

$$R_2 = \{a_0 + a_1 r + a_2 r^2 + a_3 r^3 + a_4 r^4 + a_4 r^5 + \ldots). \tag{12}$$

Then

$$\frac{1}{r}\frac{dR_2}{dr} = a_1 r^{-1} + 2a_2 + 3a_3 r + 4a_4 r^2 + 5a_5 r^3 + \ldots \tag{13}$$

and

$$\frac{d^2R_2}{dr^2} = 2a_2 + 6a_3 r + 12a_4 r^2 + 20a_5 r^3 + \ldots \tag{14}$$

Substitute equations (12), (13), (14) into equation (11)

$$2a_2 + 6a_3 r + 12a_4 r^2 + 20a_5 r^3 + a_1 r^{-1} + 2a_2 + 3a_3 r + 4a_4 r^2 + 5a_5 r^3 - a_0 r^{-2} - a_1 r^{-1} - a_2 - a_3 r - a_4 r^2 - a_5 r^3 - a_0 k^2 - a_1 r k^2 - a_2 k^2 r^2 - a_3 k^2 r^3 - a_4 k^2 r^4 - \ldots = A\, I_1(kr) \tag{15}$$

$$I_1(kr) = \frac{1}{2}kr + \frac{1}{16}k^3 r^3 + \frac{1}{384}k^5 r^5 + \ldots$$

$$2a_2 + 6a_3r + 12a_4r^2 + 20a_5r^3 + a_1r^{-1} + 2a_2 + 3a_3r + 4a_4r^2 + 5a_5r^3$$
$$- a_0r^{-2} - a_1r^{-1} - a_2 - a_3r - a_4r^2 - a_5r^3 - a_0k^2 - a_1k^2r$$
$$- a_2k^2r^2 - a_3k^2r^3 - \ldots - A\frac{1}{2}kr - A\frac{1}{16}k^3r^3 - A\frac{1}{384}k^5r^5 - \ldots$$
$$= 0 \qquad (16)$$

Equate coefficients in equation (16)

$$r^{-2} \rightarrow \quad \underline{-a_0 = 0} \qquad (17)$$

$$r^{-1} \rightarrow \quad a_1 - a_1 = 0 \qquad (18)$$

$$r^0 \rightarrow \quad 2a_2 + 2a_2 - a_2 - a_0k^2 = 0 \qquad (19)$$
$$3a_2 - a_0k^2 = 0$$
$$\underline{a_2 = 0}$$

$$r^1 \rightarrow \quad 6a_3 + 3a_3 - a_3 - a_1k^2 - A\frac{1}{2}k = 0 \qquad (20)$$
$$8a_3 - a_1k^2 - A\frac{1}{2}kr = 0$$
$$a_3 = \frac{a_1k^2 + A\frac{1}{2}k}{8}$$

$$r^2 \rightarrow \quad 12a_4 + 4a_4 - a_4 - a_2k^2 = 0 \qquad (21)$$
$$15a_4 = 0$$
$$\underline{a_4 = 0}$$

$$r^3 \rightarrow \quad 20a_5 + 5a_5 - a_5 - a_3k^2 - A\frac{1}{16}k^3 = 0 \qquad (22)$$
$$24a_5 = a_3k^2 + A\frac{1}{16}k^3$$
$$a_5 = \frac{\frac{1}{8}a_1k^4 + A\frac{1}{16}k^3 + A\frac{1}{16}k^3}{24}$$
$$\underline{a_5 = \frac{a_1k^4}{192} + \frac{Ak^3}{192}}$$

Place equations (17) through (22) into equation (12)

$$R_2 = a_1 r + \left(\frac{a_1 k^2}{8} + \frac{Ak}{16}\right) r^3 + \left(\frac{a_1 k^4}{192} + \frac{Ak^3}{192}\right) r^5 + \ldots \tag{23}$$

Let

$$a_1 = \frac{1}{2}$$

$$R_2 = \frac{1}{2} r + \left(\frac{k^2}{16} + \frac{Ak}{16}\right) r^3 + \left(\frac{k^4}{384} + \frac{2Ak^3}{384}\right) r^5 + \ldots \tag{24}$$

Let

$$A = 2k \quad .$$

Then

$$R_2 = \frac{1}{2} r + \frac{3}{16} k^2 r^3 + \frac{5}{384} k^4 r^5 + \ldots \tag{25}$$

or

$$R_1 = \frac{d}{dk} I_1(kr) \quad . \tag{26}$$

It can also be shown that

$$R_2 = \frac{d}{dk} K_1(kr) \tag{27}$$

APPENDIX B

DIAZO SOLUTION AND PRINTING PROCESS

Initially a thin sheet was molded. Its thickness was approximately 0.03 inches. It was made of Solithane 113 according to the description given in Section **3.2.** The surfaces of the sheet were cleaned thoroughly with a solvent.

A very thin layer of white latex paint, mixed with liquid rubber latex, was sprayed on one surface of the thin sheet. The rubber latex was mixed with the paint in order to give the paint extensibility without cracking when the thin sheet was stretched. The purpose of the mixture was to provide a good contrasting background **for** the dark lines of the grid.

Diazo printing, though not good for general photographic purposes, is, however, very good when reproduction of lines is needed. Therefore, the diazo process is readily adaptable for the application of grid lines to the surface of solid fuel propellants. Also, the diazo process was chosen because the solutions used in more conventional printing processes react chemically with Solithane.

The painted surface of the thin sheet was coated with a diazo-type photosensitive solution which contained the following proportion of chemicals (for a 100 c.c. water solution):

Glycol	3.0 c.c.
Thiourea	4.5 g.
Citric Acid.	4.0 g.
Recorcinol	0.3 g.
Zinc Chloride. . . .	4.5 g.

Coupler III*. . . .	2.0 g.
Diazo #8**	1.0 g.
Diazo #9***	1.0 g.

After sufficient drying time, approximately three days, the sheet was placed in a vacuum printing frame with a photographic negative superposed on it. The photographic negative was of the desired grid pattern. The printing frame was used in order to insure intimate contact between the sheet and the negative. Illumination of the thin sheet with an ultra-violet light source for an appropriate amount of time destroyed the diazo salt which was not covered by the lines of the photographic negative. Ammonia vapor was used to develop the unexposed portions of the diazo salt on the sheet.

---

*These are trade names of the materials of the Andrews Paper and Chemical Co., Port Washington, N.Y. Their chemical designations follow.

Coupler III is 2,3 dyhydroxy naphthalene-6-sulfonic acid sodium salt.

**Diazo #8 is para diazo NN dimethyl aniline 1/2 zinc chloride salt.

***Diazo #9 is para diazo NN diethyl aniline zinc chloride salt.

APPENDIX C

Sample Analysis of Moiré Fringes

An example of the formation of moiré fringes is shown in Figure 16. The picture shown is a close-up of the fringes formed on a tension specimen, photographed when a load of 0.6 pounds had been applied to the specimen. The method of analysis of such a set of fringes is presented in section 3.4, Moire Fringe Theory.

A plot of accumulated fringe distance versus fringe number is presented in Figure 17. This plot was made, as directed in section 3.4, from the picture of the moiré fringes. Since the picture is a magnification of the original fringes, a factor of reduction must be included in the calculations of strains or extension ratios made from the data acquired from the plot of accumulated fringe distance versus fringe number.

The modulus of the material tested was determined from a plot of true stress, $\sigma_t = \left(\frac{P}{A}\right)\lambda$, versus extension ratio, λ. In the above equations, P is the load applied to the specimen, A is the original cross-sectional area of the specimen, and h is the extension ratio. The slope of this plot was taken to be the modulus of the material.

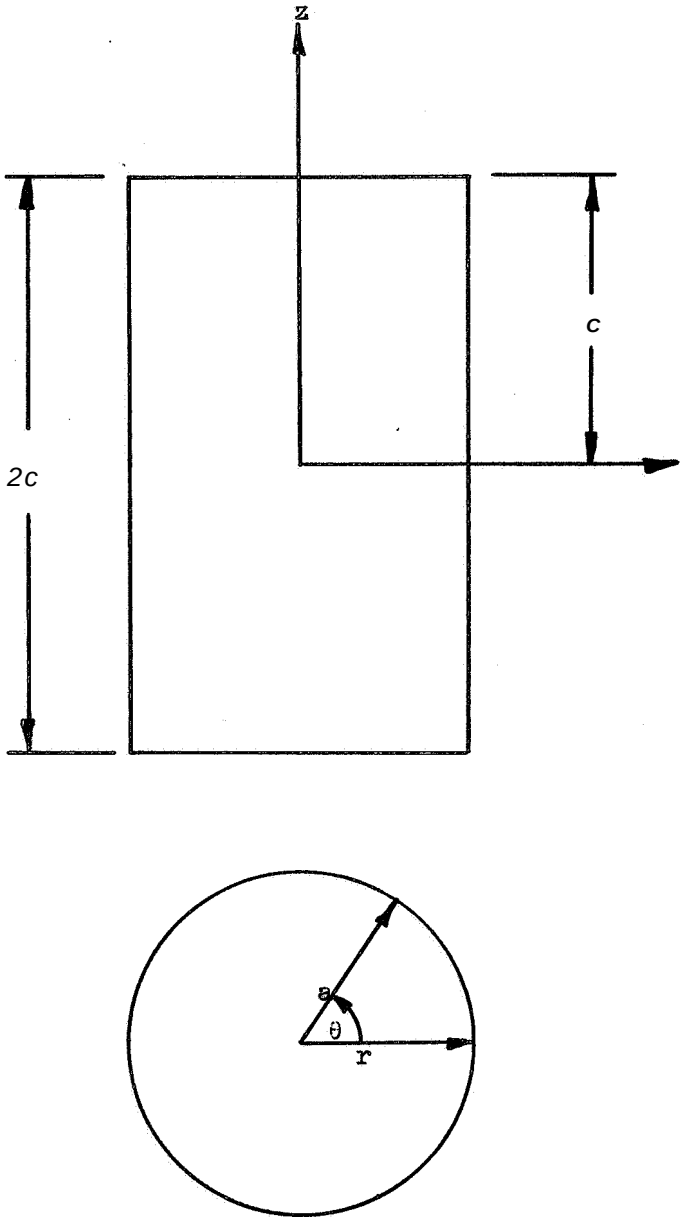

Fig. 1 Definition of Coordinate System used in Theoretical Derivations,

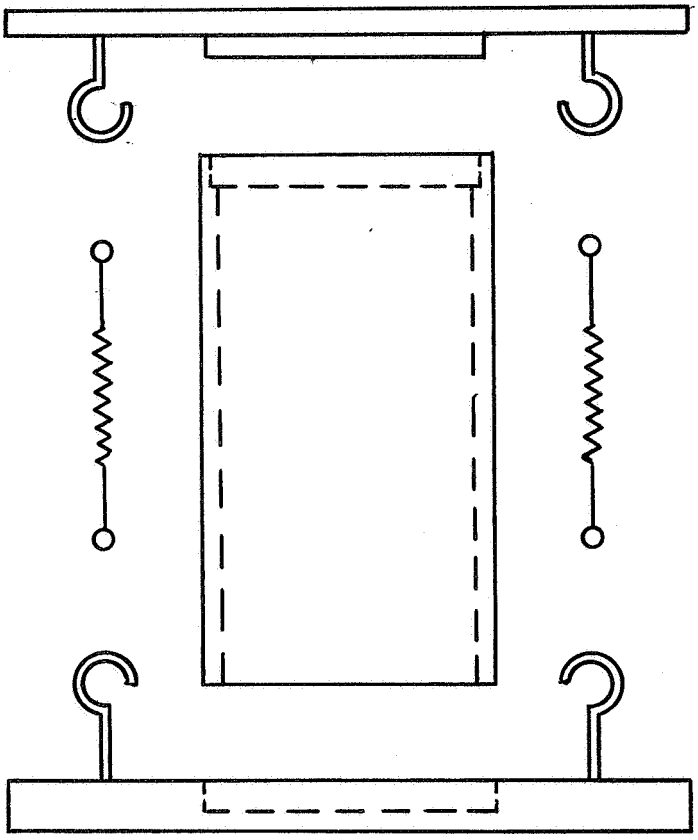

Fig. 2 Molds for Casting Cylindrical Specimens.

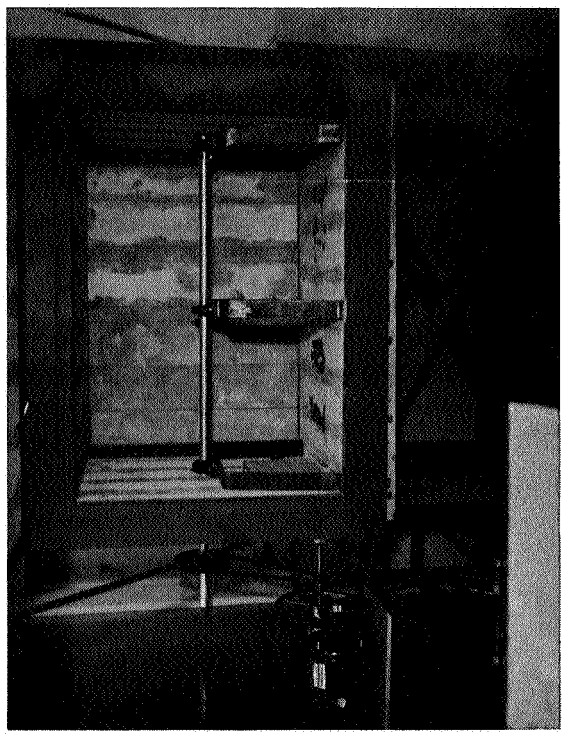

Figure 3. Curing Oven.

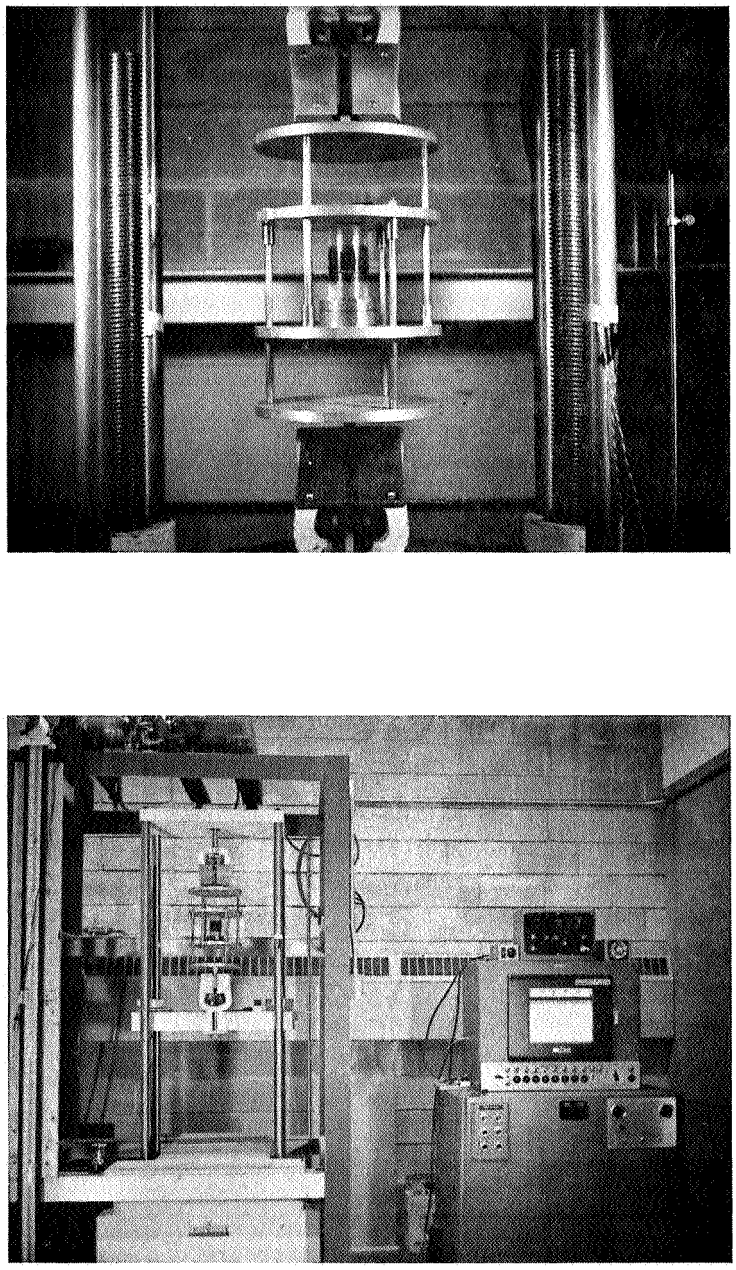

Figure 4. Tinius Olsen Testing Machine with Compression Apparatus Installed.

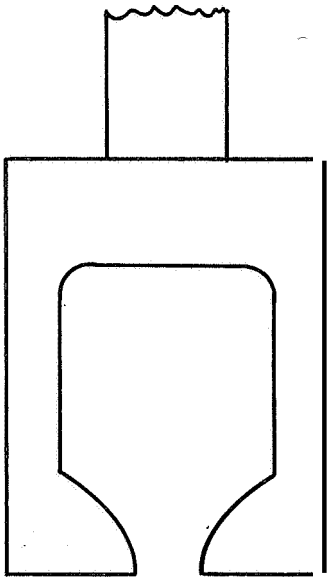

Fig. 6 Tension Specimen Grips.

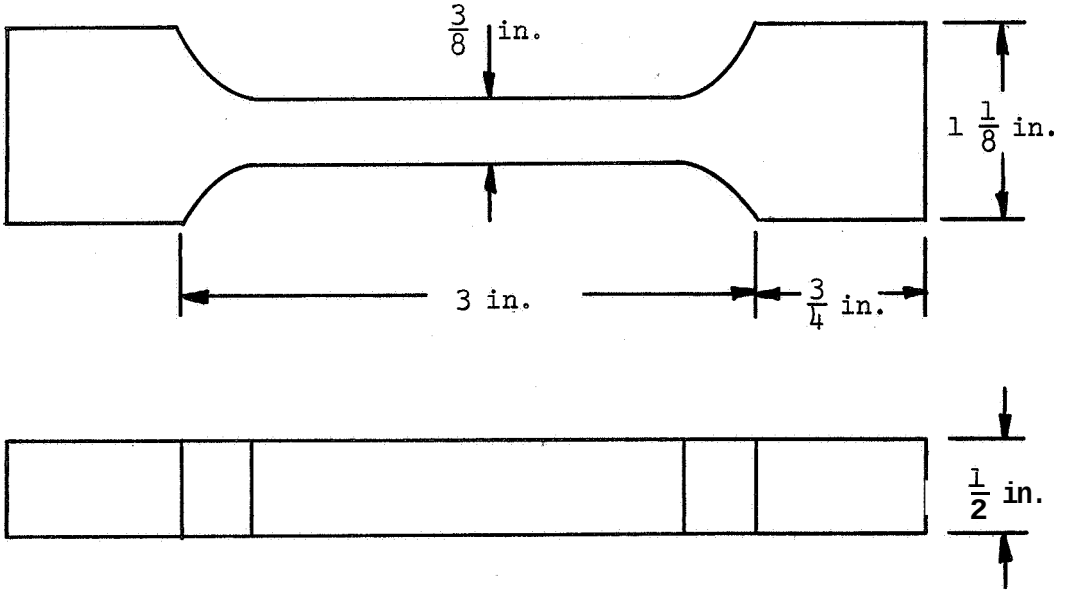

Fig. 5 Tension Specimen,

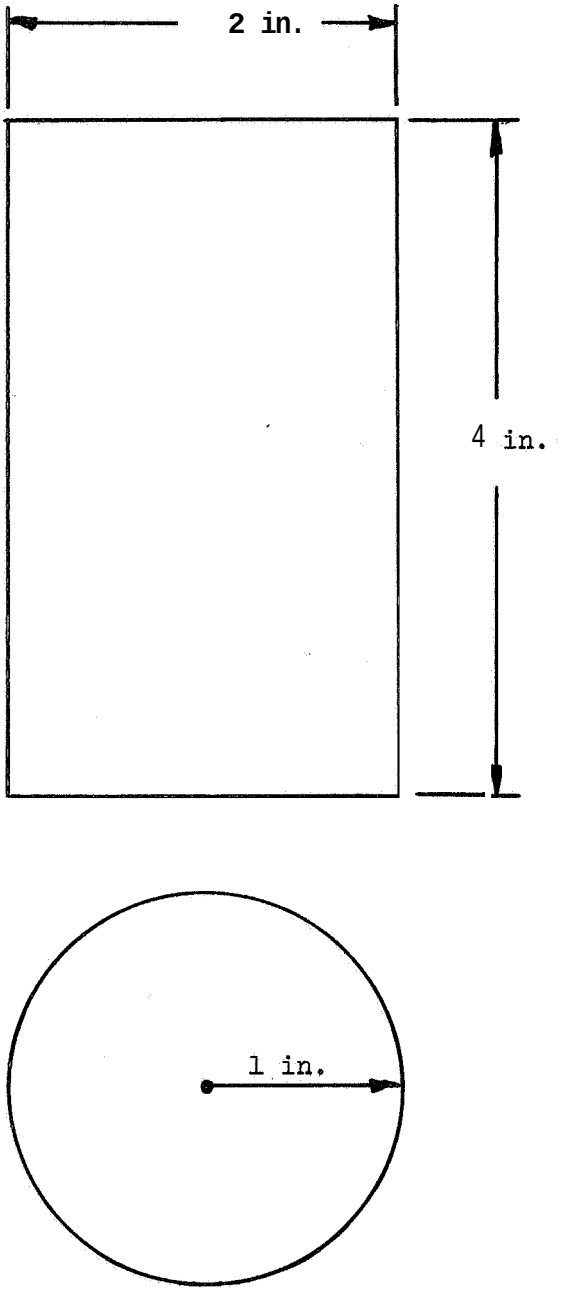

Fig. 7 Compression Specimen.

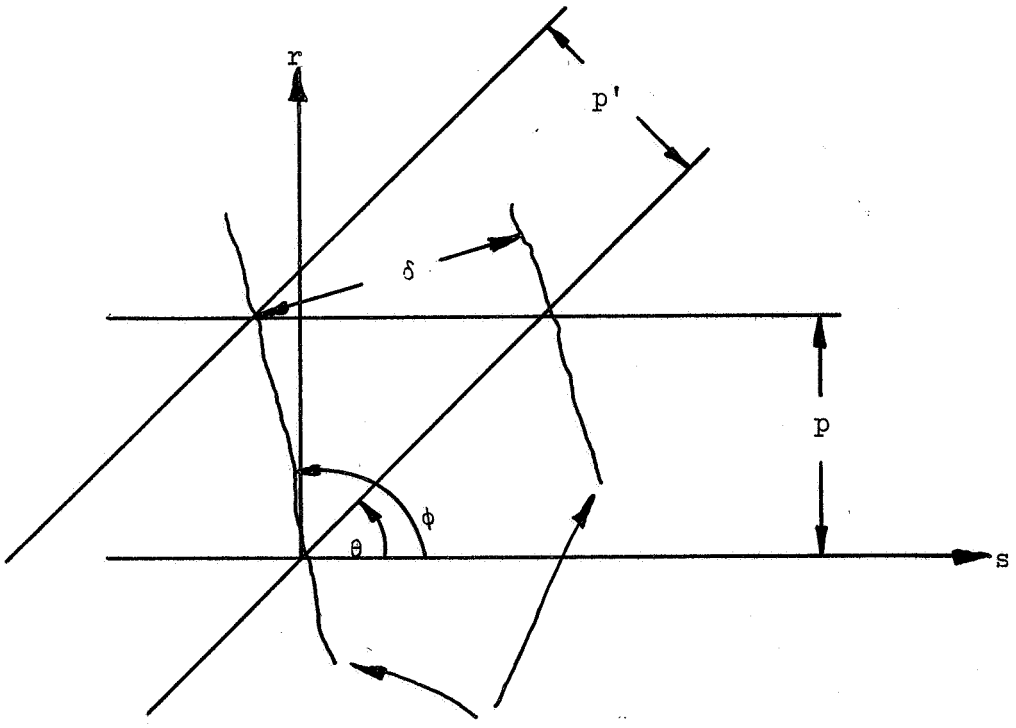

Fig. 8 Close Up of Formation of Moiré Fringes.

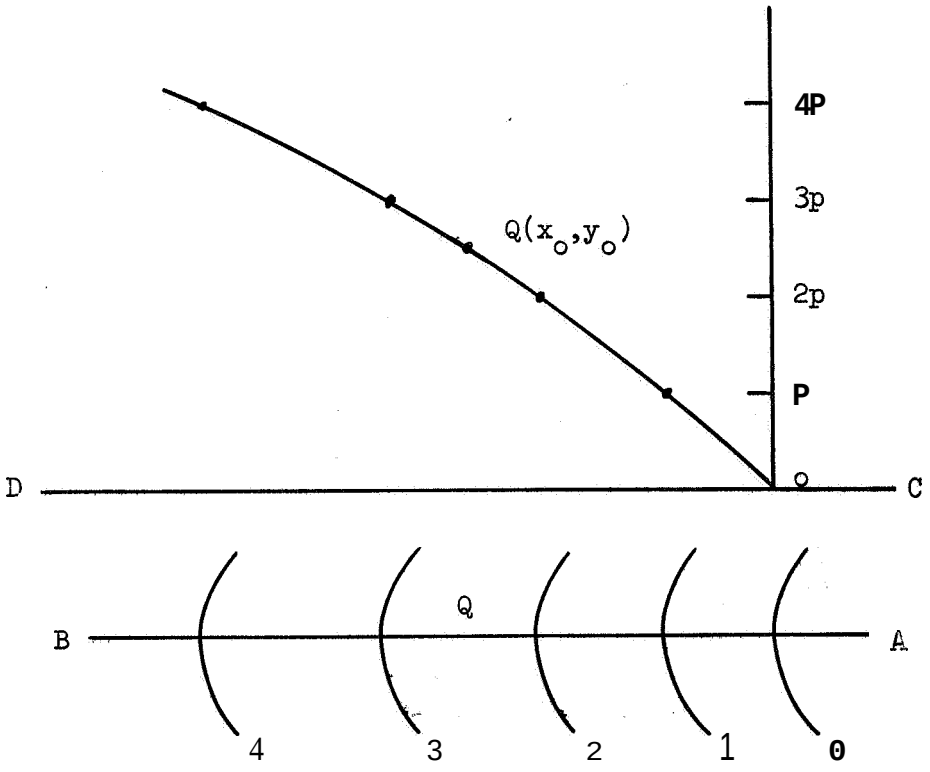

Fig. 9 Moiré Fringe Analysis by Displacement Method.

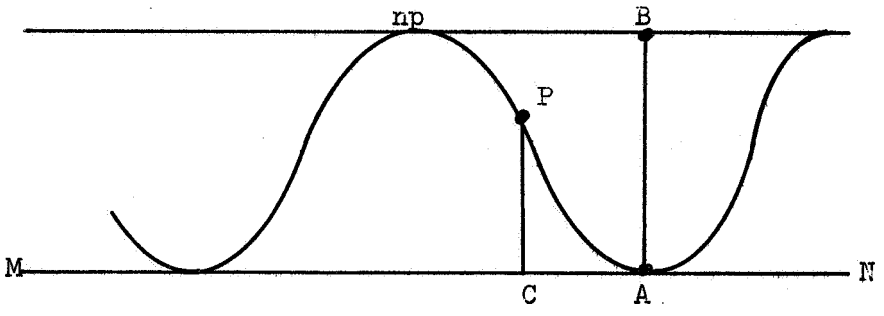

Fig. 10 Sample Output of Photocell Equipment of Light Intensity Method.

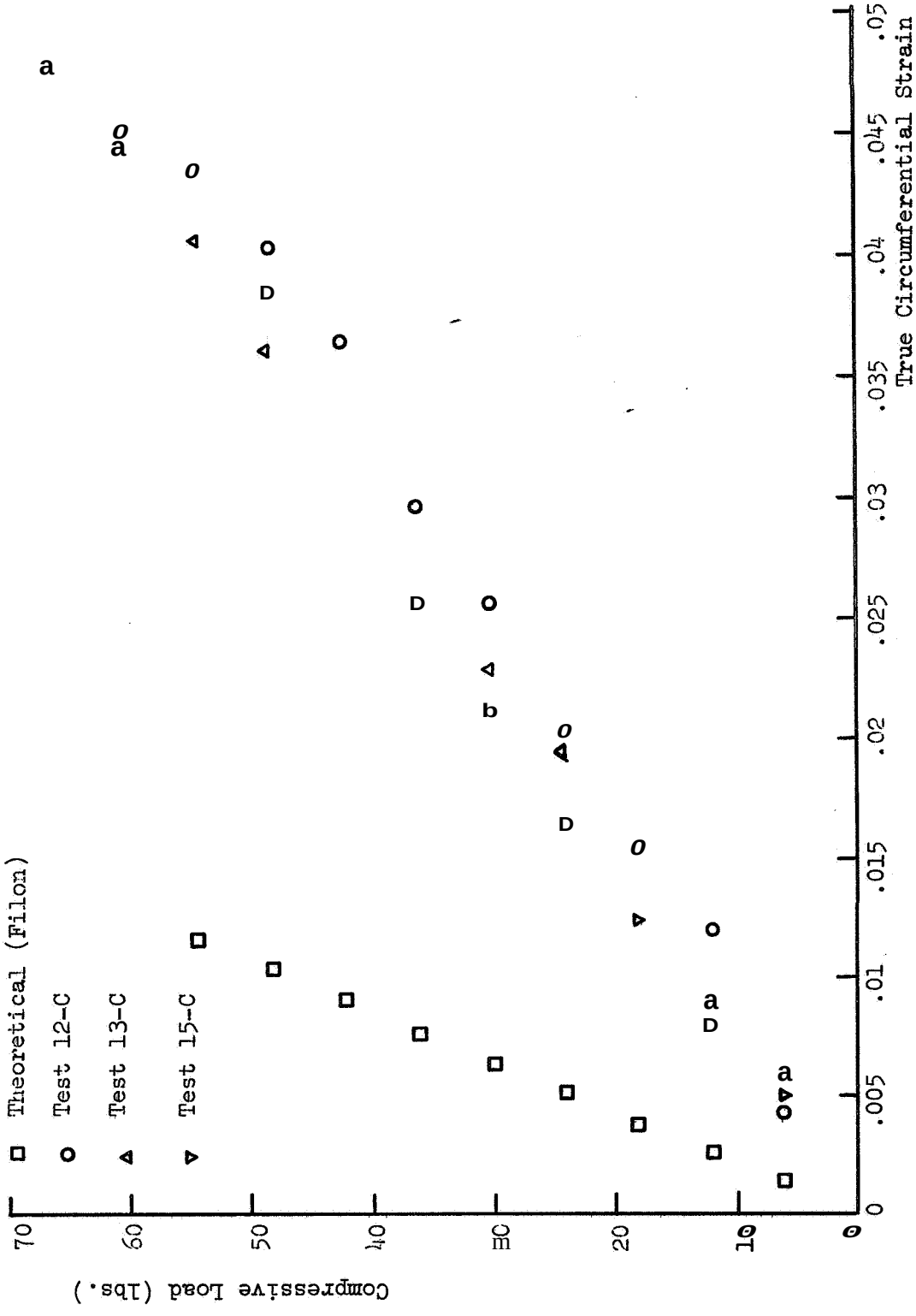

Fig. 11 Compressive Load Versus True Circumferential Strain for Non-Lubricated Ends.

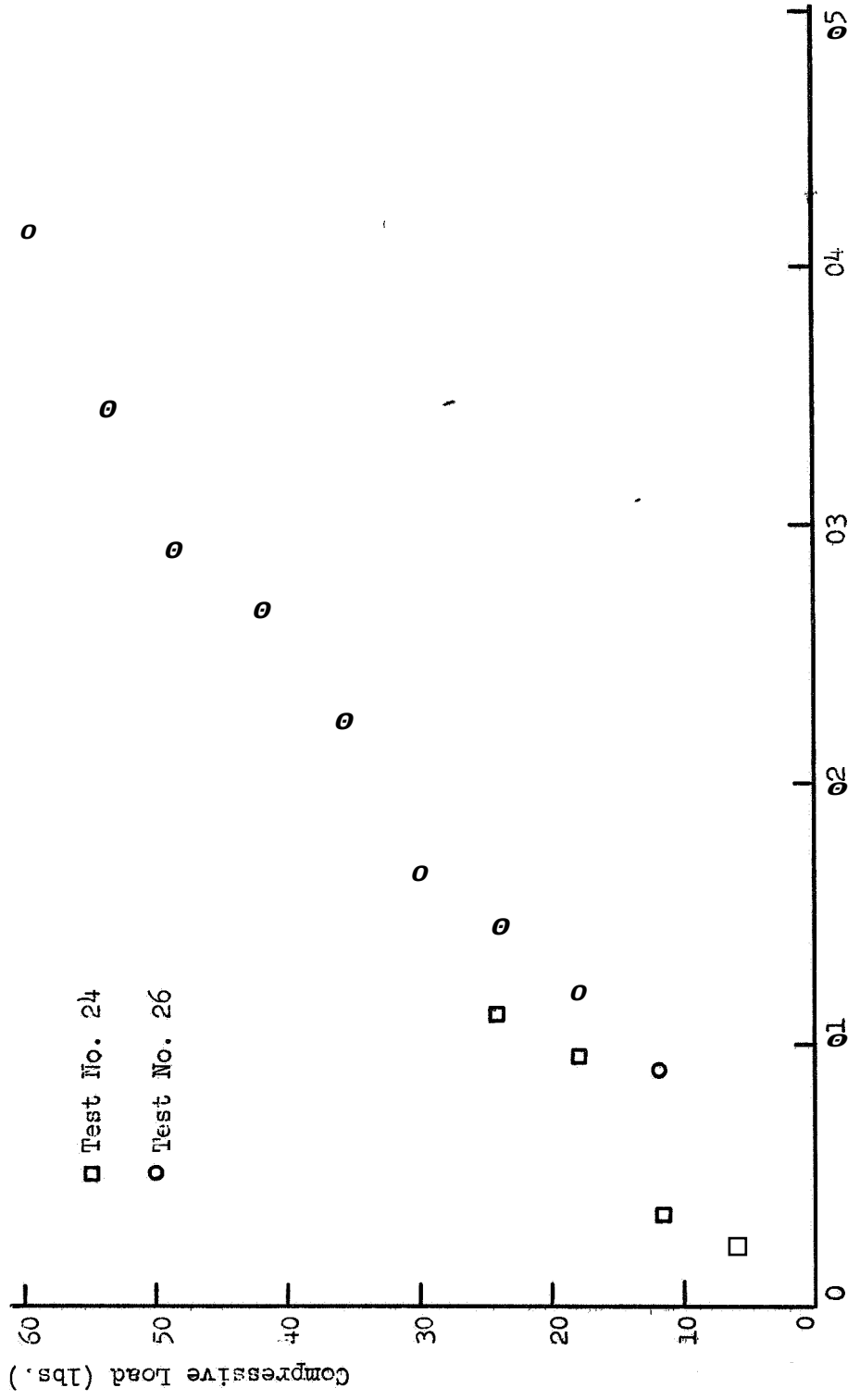

Fig. 12 Compressive Load Versus True Circumferential Strain for Lubricated Ends.

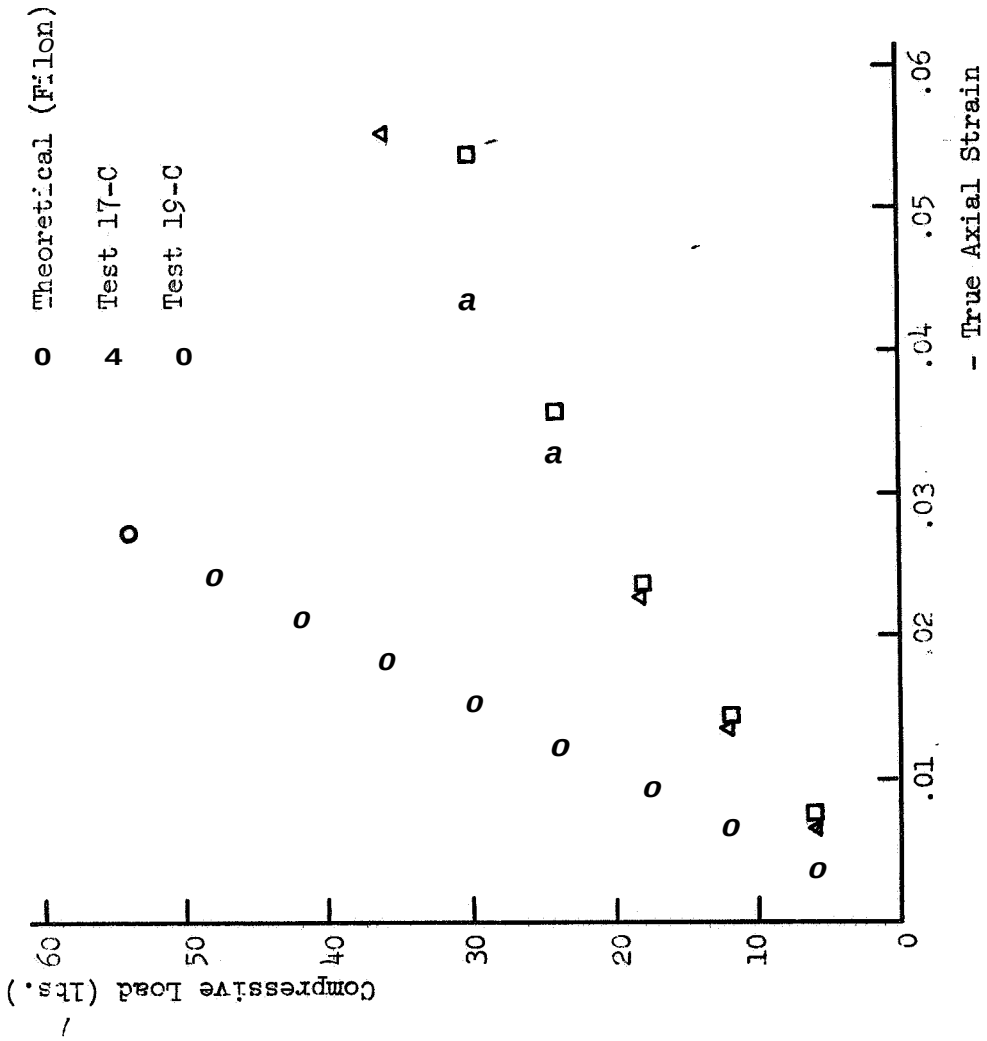

Fig. 13 Compressive Load Versus True Axial Strain for Non-Lubricated Ends.

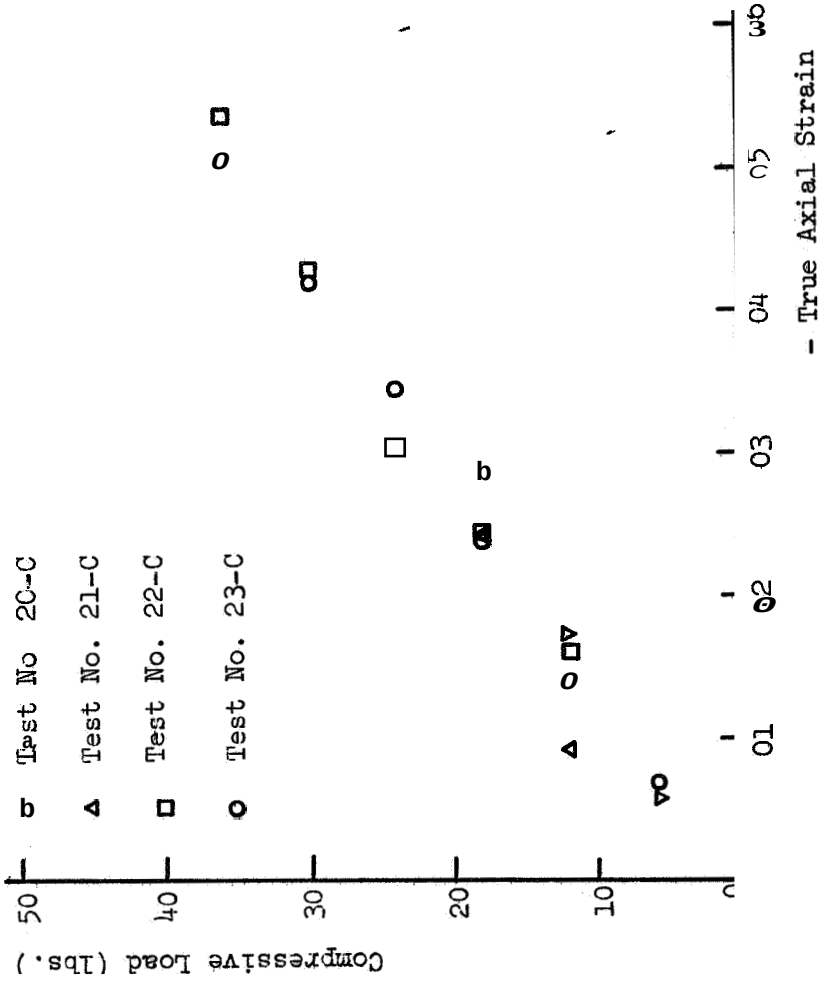

Fig. 14 Compressive Load Versus True Axial Strain for Lubricated Ends.

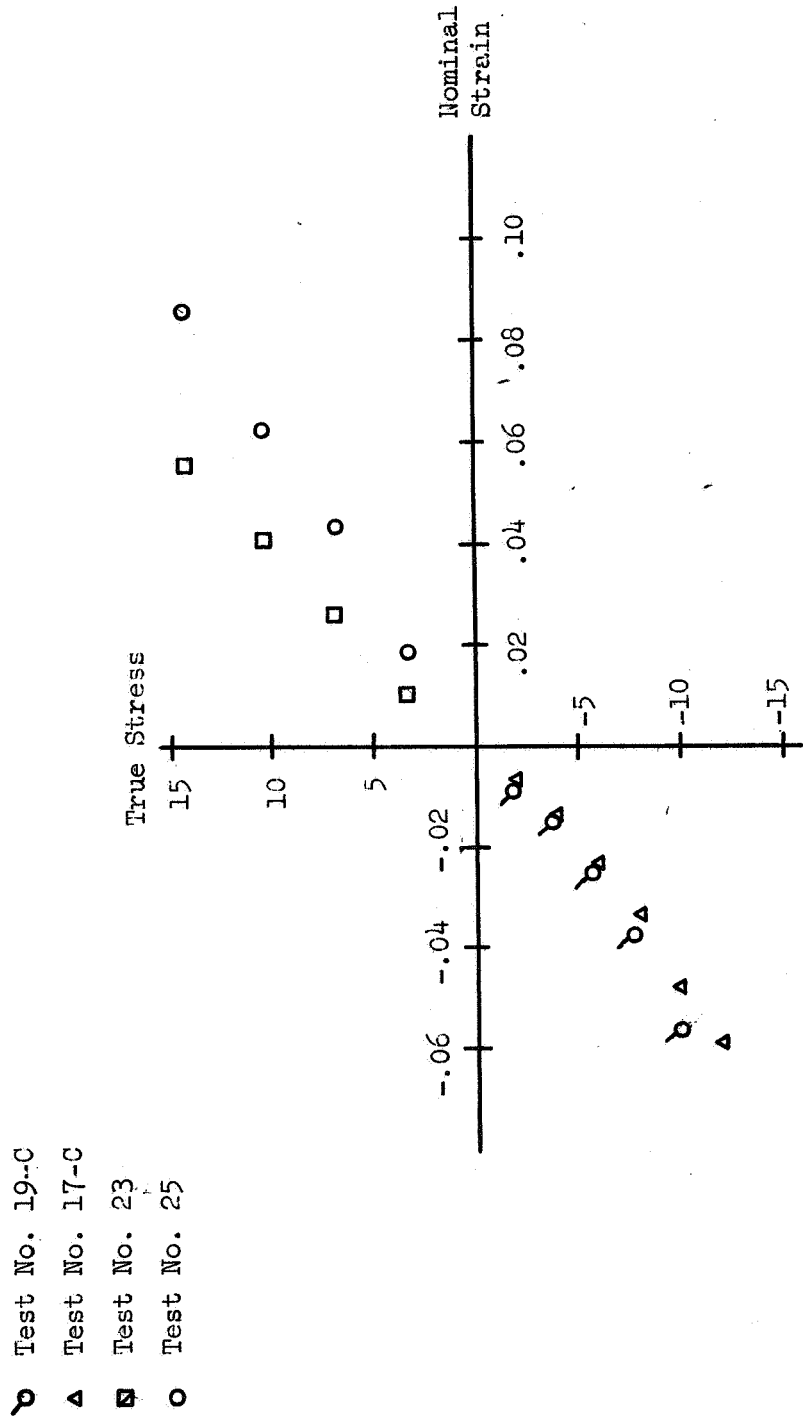

Fig. 15 True Stress Versus Nominal Strain

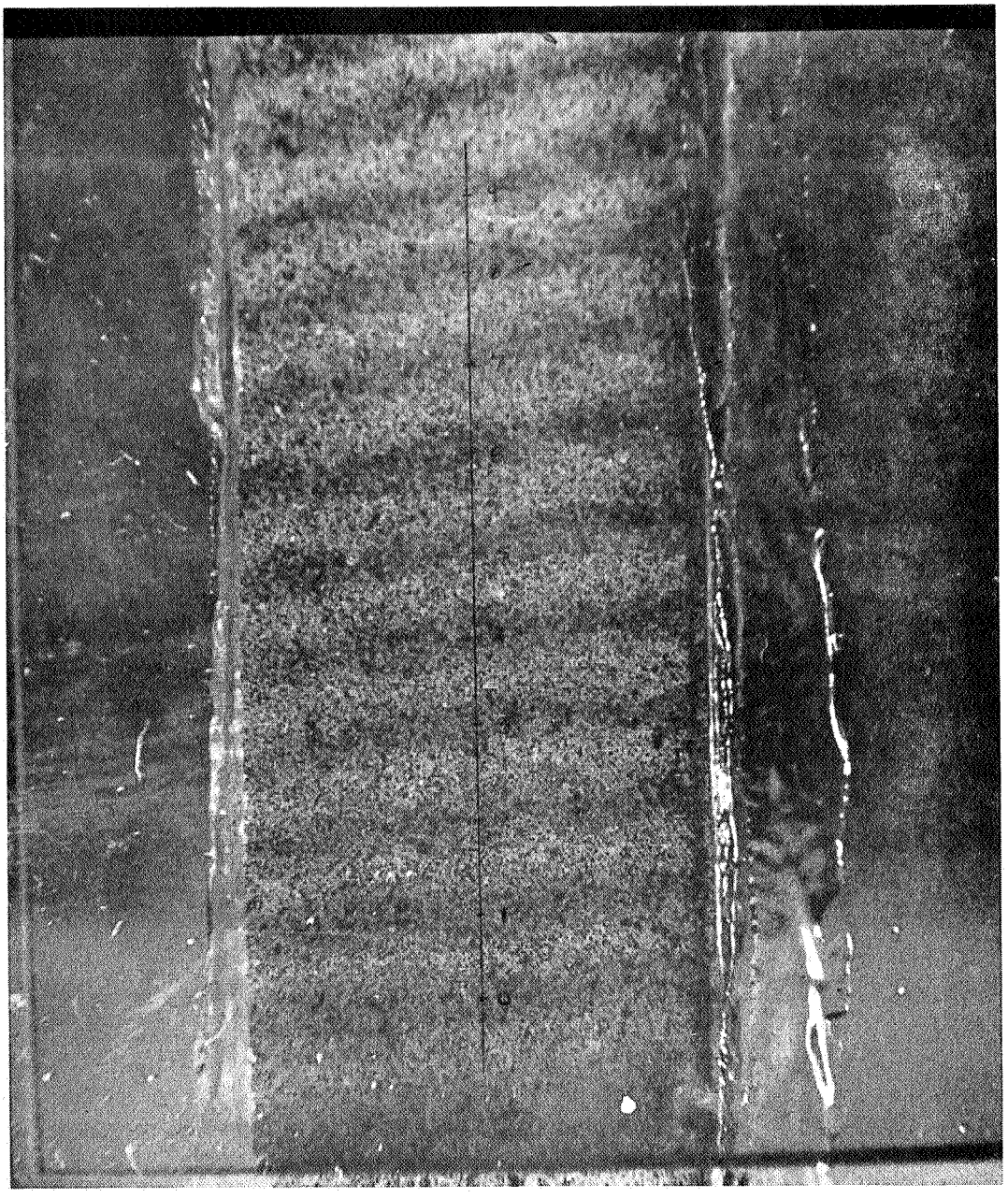

Figure 16. Moiré Fringes.

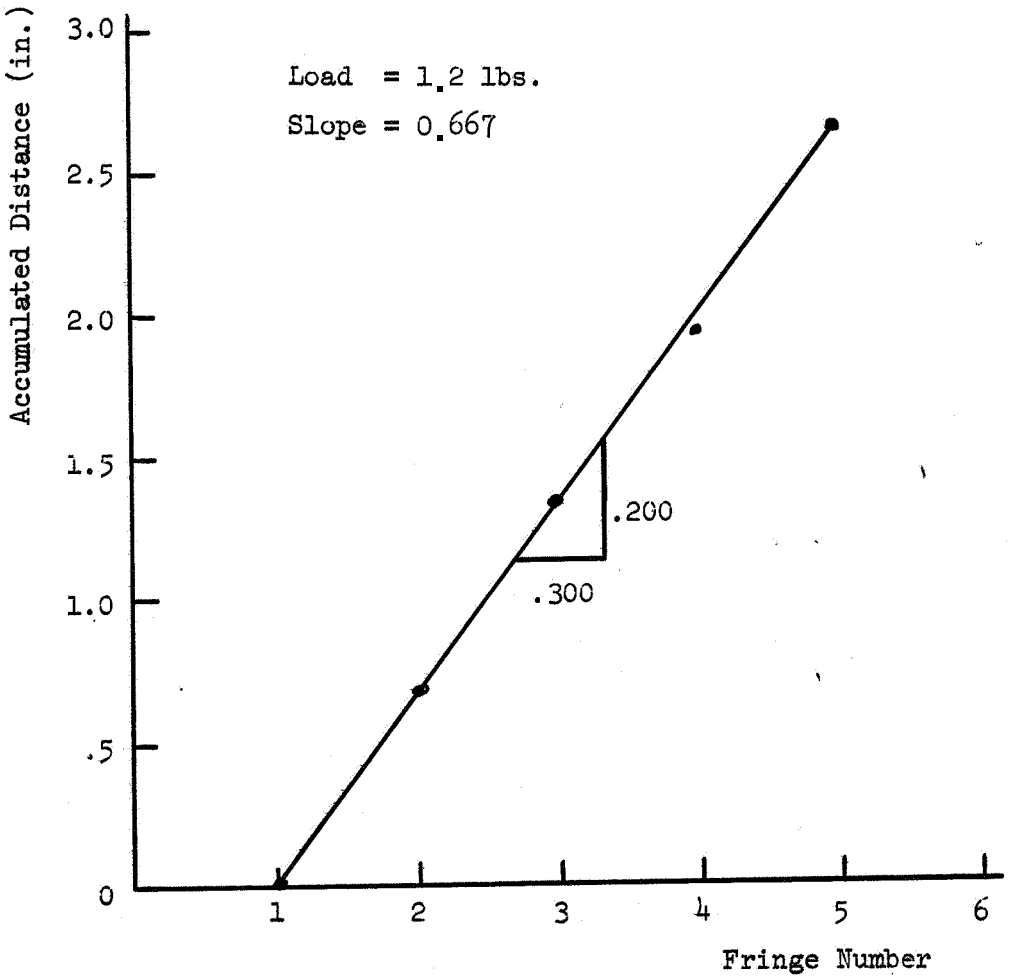

Fig. 17 Accumulated Fringe Distance Wersus Fringe Number

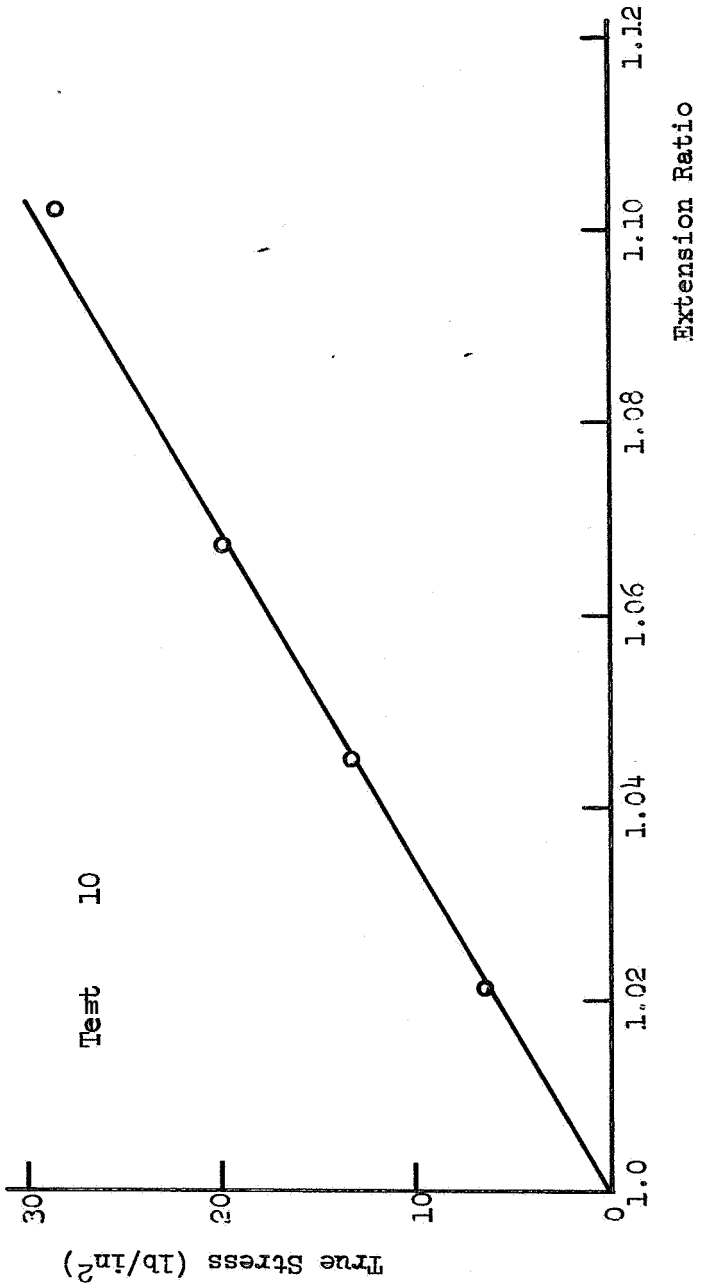

Fig. 18 True Stress Versus True Strain for Determination of Modulus.